

Chapter 2: Cell-Selective Biological Activity of Rhodium Metalloinsertors Correlates with Subcellular Localization**

2.1 Introduction

The mismatch repair (MMR) machinery recognizes and repairs single base lesions and mismatches that arise from errors in DNA replication.^{1,2} Deficiencies in the MMR machinery increase the rate of mutagenesis 50-1000 fold, resulting in an enhanced susceptibility to cancer.^{3,4} Additionally, many MMR-deficient cancers exhibit resistance to chemotherapeutics such as DNA alkylators and platinating agents,⁵ as MMR proteins are responsible for recognizing the DNA adducts formed by these agents.⁶ As a strategy to target MMR-deficient cancers, we have developed a variety of bulky rhodium complexes that target DNA mismatches through metalloinsertion, a binding mode in which a sterically expansive ligand, such as chrysenequinone diimine (chrysi), inserts into the DNA base stack at the site of the mismatch and ejects the thermodynamically destabilized bases. These complexes exhibit 1000-fold selectivity over well-matched DNA and target 80% of all mismatches irrespective of sequence context.⁷⁻¹⁰

Metalloinsertion represents a general binding mode for the binding of bulky metal complexes to destabilized mismatches. With intercalative binding, well-matched,

Adapted from Weidmann, A. G., Komor A. C., Barton, J. K. "Biological Effects of Simple Changes in Functionality on Rhodium Metalloinsertors." *Philos. Trans. R. Soc. A.* **2013, 371, 20120117; and Komor, A. C.; Schneider, C. J.; Weidmann, A. G.; Barton, J. K. "Cell-Selective Biological Activity of Rhodium Metalloinsertors Correlates with Subcellular Localization." *J. Am. Chem. Soc.* **2012**, 134, 19223-19233. © 2012 American Chemical Society.

Acknowledgements: Alexis Komor synthesized $[\text{Rh}(\text{phzi})(\text{NH}_3)_4]^{3+}$, $[\text{Rh}(\text{bpy})_2\text{chrysi}]^{3+}$, $[\text{Rh}(\text{HDPA})_2\text{chrysi}]^{3+}$, and $[\text{Rh}(\text{DIP})_2\text{chrysi}]^{3+}$ complexes, and Curtis Schneider synthesized the $[\text{Rh}(\text{chrysi})(\text{phen})(\text{L})]\text{Cl}_3$ (L= HDPA, MeDPA, PrDPA) compounds. I synthesized $[\text{Rh}(\text{DPAE})_2\text{chrysi}]^{3+}$, $[\text{Rh}(\text{PrDPA})_2\text{chrysi}]^{3+}$, and the corresponding ligands, and also assisted in the ELISA, MTT, and ICP-MS (cellular uptake and nuclear and mitochondrial localization) biological experiments.

hydrogen-bonded base pairs separate, increasing the helical pitch, so that an aromatic heterocyclic ligand can stack within the DNA duplex, essentially like another base pair.¹¹ For metalloinsertion, the flat aromatic heterocyclic ligand is simply too large to insert easily into the DNA duplex and instead, to accommodate the inserting ligand, the base pairs must separate and be ejected from the helix.^{12,13} This ejection only occurs easily at destabilized mismatched sites, and thus the binding affinity for mismatches correlates with the thermodynamic instability of the mismatch, the ease of separation and ejection. Several crystal structures have shown that metalloinsertion occurs from the minor groove side with no increase in helical pitch.¹²⁻¹⁴ As a result, for the tris(chelate) metalloinsertors, binding within the small minor groove is highly enantioselective for the D-isomer.

Previously, we have demonstrated that, because of this high specificity for DNA mismatches, these rhodium metalloinsertors have unique biological properties.¹⁵⁻¹⁷ Their biological activity has been characterized in two isogenic cell lines derived from human colorectal carcinoma (HCT116), one MMR-deficient (HCT116O), the other MMR-proficient (HCT116N). The HCT116 parent cell line is a human colorectal carcinoma line deficient in the *hMLH1* gene. This gene encodes for part of the mismatch repair (MMR) machinery; consequently this cell line is MMR deficient. The HCT116N cell line has been transfected with human chromosome 3 (ch3), which restores MMR proficiency, while the HCT116O cell line has been transfected with human chromosome 2 (ch2), leaving it MMR deficient.¹⁸ Cellular proliferation assays have shown that our rhodium metalloinsertors exhibit antiproliferative activity preferentially in the MMR-deficient HCT116O line. Moreover, the extent of this cell-selectivity is dependent on binding of

the complex to a mismatched site: the higher the mismatch binding affinity, the greater the differential inhibition of cellular proliferation in MMR-deficient versus proficient cells.¹⁶ Recently, complexes prepared with more efficient cellular uptake have also shown a differential cytotoxicity in MMR-deficient versus proficient cells.¹⁷ The results therefore support the strategy of a cell-selective chemotherapeutic strategy based upon DNA mismatch targeting.

In the development of novel metalloinsertors for improved cell-selective antiproliferative activity, two complexes were discovered to have strikingly different biological activities, despite containing only minor functional group changes to their overall structure. The complexes, depicted in **Figure 2.1**, are tris(chelate) compounds that consist of two *N*-functionalized dipyridylamine (DPA) ligands in addition to the inserting chrysi ligand. The modified DPA ligands contain either ethanol or *N*-propyl moieties, affording $[\text{Rh}(\text{DPAE})_2\text{chrysi}]^{3+}$ (**1a**) and $[\text{Rh}(\text{PrDPA})_2\text{chrysi}]^{3+}$ (**1b**), respectively. $[\text{Rh}(\text{DPAE})_2\text{chrysi}]^{3+}$ exhibits exceptional inhibition of growth selectively in MMR-deficient cells, whereas $[\text{Rh}(\text{PrDPA})_2\text{chrysi}]^{3+}$ displays little detectable cell-selectivity; instead the PrDPA complex inhibits cellular proliferation in both cell lines. Here we explore the various factors that contribute to this cell-selective biological activity for one complex with no activity for the closely related complex. We find that the selective activity in MMR-deficient cells depends not only upon a high binding affinity for single base mismatches, present for both complexes, but also upon efficient targeting of the complexes to nuclear rather than mitochondrial DNA. Specifically, genomic DNA mismatches are implicated as the target for rhodium metalloinsertors *in cellulo*, whereas the mitochondrion appears to be an undesirable target. Furthermore, this trend was

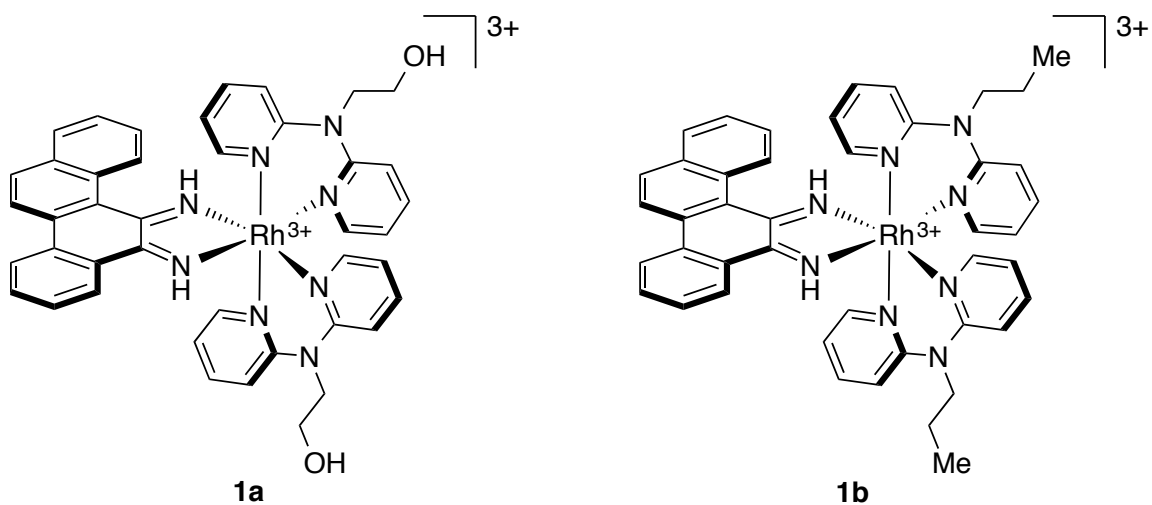


Figure 2.1 Rh(L)₂chrysi³⁺ metalloinsertors. Rh(DPAE)₂chrysi³⁺ (**1a**) contains two ethanol moieties off the central nitrogen atoms, where Rh(PrDPA)₂chrysi³⁺ (**1b**) contains instead two propyl groups. Both complexes also contain the sterically expanded 5,6-chrysenediimine (chrysi) inserting ligand, for selective binding of thermodynamically destabilized DNA mismatches.

confirmed generally in a study of a family of ten metalloinsertor complexes with similar binding affinities, but varying lipophilicities.¹⁹ These results underscore sub-cellular localization as an important factor also in therapeutic design.

2.2 Experimental Protocols

2.2.1 Materials

All organic reagents were purchased from Sigma-Aldrich unless otherwise noted. Commercially available chemicals were used as received without further purification. RhCl₃ starting material was purchased from Pressure Chemical Co. Media and supplements were purchased from Invitrogen (Carlsbad, CA). BrdU, antibodies, and buffers were purchased in kit format from Roche Molecular Biochemical (Mannheim, Germany).

Oligonucleotides were ordered from Integrated DNA Technologies and purified by HPLC using a C18 reverse-phase column (Varian, Inc). All HPLC purifications were carried out on a Hewlett-Packard 1100 HPLC. DNA purity was confirmed by MALDI-TOF mass spectrometry and quantified by UV-vis using the extinction coefficients at 260 nm estimated for single-stranded DNA. UV-vis characterizations were performed on a Beckmann DU 7400 spectrophotometer.

2.2.2 Ligand Synthesis (Scheme 2.1)

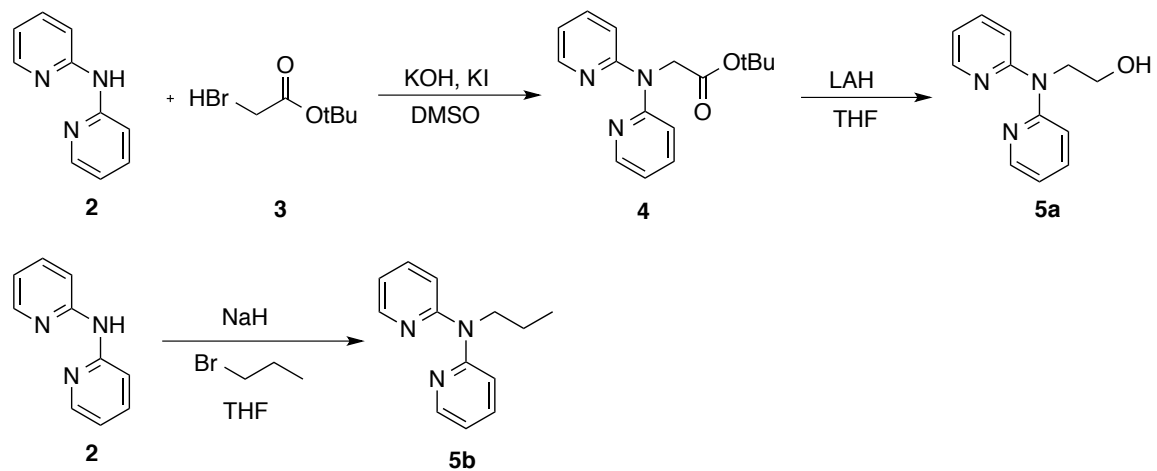
The ancillary ligands, 2-(di(pyridin-2-yl)amino)ethanol (DPAE, 5a) and *N*-propyl-*N*-(pyridin-2-yl)pyridin-2-amine (PrDPA, 5b), were synthesized from 2,2'-dipyridylamine (2) according to Scheme 1.

2.2.2.1 Tert-butyl 2-(di(pyridine-2-yl)amino)acetate (4). Tert-butyl 2-(di(pyridine-2-yl)amino)acetate (4) was prepared according to a modified literature

procedure.²⁰ Potassium hydroxide (3.0 g, 53.6 mmol, 4.6 equiv) was added to a solution of 2,2'-dipyridylamine (**2**) (2.0 g, 11.7 mmol) in 40 ml DMSO and stirred at room temperature for 16 h. Potassium iodide (200 mg, 1.2 mmol, 0.1 equiv) and tert-butyl bromoacetate (**3**) (4 ml, 2.3 equiv) were added to the mixture, and the reaction was stirred for 2 h at room temperature. The reaction mixture was extracted with diethyl ether (3 x 50 ml). The organic fractions were combined and dried over magnesium sulfate, and the solvent was removed by rotary evaporation. The crude product was isolated by flash chromatography (SiO₂, hexane/ethyl acetate = 8:2) to give a yellow oil. Yield: 2.92 g (88%). ¹H NMR (CDCl₃, 300 MHz): δ 8.33 (ddd, J = 5.0, 1.9, 0.9 Hz; 2H), 7.53 (m, 2H), 7.23 (m, 2H), 6.88 (ddd, J = 7.2, 5.0, 0.9 Hz; 2H), 4.84 (s, 2H), 1.42 (s, 9H). ESI-MS (cation): 286 m/z (M + H⁺) obsd, 286 m/z calcd.

2.2.2.2 2-(di(pyridine-2-yl)amino)ethanol (5a). To a slurry of LAH (1.17 g, 30.8 mmol, 3.0 equiv) in THF (45 ml) was added **4** (2.9 g, 10.2 mmol) at 0 °C under 1 atm Ar. The reaction was slowly warmed to room temperature over 4 h. The reaction mixture was then diluted with ethyl ether and cooled to 0 °C. The reaction was quenched via careful addition of water (4.0 ml) and then dried with magnesium sulfate. The solvent was removed in vacuo, and the crude product was purified by flash chromatography (SiO₂, hexane/ethyl acetate = 1:1) to afford DPAAE (**5a**) as a pale yellow oil. Yield: 1.2 g (55%). ¹H NMR (DMSO-d₆, 300 MHz): δ 8.27 (m, 2H), 7.62 (m, 2H), 7.16 (d, J = 8.4 Hz, 2H), 6.93 (m, 2H), 4.92 (t, J = 5.4 Hz, 1H), 4.16 (t, J = 6.5 Hz, 2H), 3.58 (q, J = 6.5 Hz, 2H). ESI-MS (cation): 216.1 m/z (M + H⁺) obsd, 215 m/z calcd.

2.2.2.3 N-propyl-N-(pyridin-2-yl)pyridin-2-amine (5b). To a slurry of sodium hydride (70 mg, 2.9 mmol) in THF (10 ml) was added **2** (500 mg, 2.9 mmol) in 5



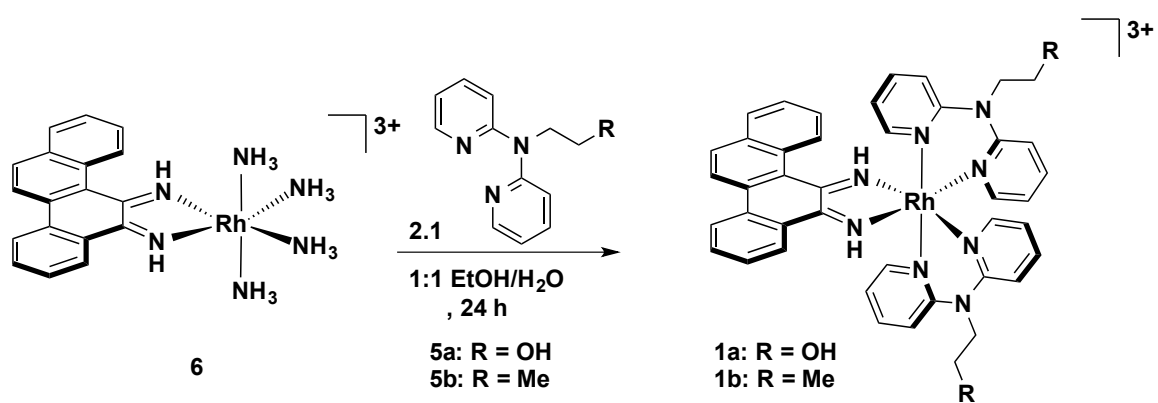
Scheme 2.1 Synthesis of ancillary ligands 2-(di(pyridine-2-yl)amino)ethanol (DPAE, **5a**) and N-propyl-N-(pyridin-2-yl)pyridin-2-amine (PrDPA, **5b**) from 2,2'-dipyridylamine (**2**).

ml THF at 0 °C under 1 atm Ar. The reaction was purged with argon for 15 min, and 1-bromopropane (468 mg, 3.8 mmol) was added dropwise and warmed to room temperature. The reaction was stirred an additional 18 h under argon at reflux temperature. The reaction mixture was extracted with dilute sodium bicarbonate, and the aqueous phase was extracted with CH₂Cl₂ (3 x 40 ml). The organic fractions were combined and dried over magnesium sulfate, and the solvent was removed *in vacuo*. **5b** was purified via flash chromatography (SiO₂, hexane/ethyl acetate = 9:1). Yield: 100 mg (25%) ¹H NMR (CDCl₃, 300 MHz): δ 8.34 (d, J = 7.7 Hz, 2H), 7.57 – 7.45 (m, 2H), 7.06 (d, J = 0.7 Hz, 2H), 6.90 – 6.79 (m, 2H), 4.19 – 4.07 (m, 2H), 1.79 – 1.65 (m, 2H), 0.99 – 0.85 (m, 3H) ppm. ESI-MS (cation): 214.1 m/z (M + H⁺) obsd, 213 m/z calcd.

2.2.3 Metal Complexes

2.2.3.1 Rh(NH₃)₄chrysi³⁺ (6**).** Rhodium precursor **6** was synthesized from Rh(NH₃)₅Cl²⁺ according to published protocols.¹⁶ The remaining complexes in this study were synthesized as described in Reference 19.** The syntheses of [Rh(DPAE)₂chrysi]³⁺ (**1a**) and [Rh(PrDPA)₂chrysi]³⁺ (**1b**) are depicted in **Scheme 2.2**.

2.2.3.2 *rac*-Rh(DPAE)₂chrysi³⁺ (1a**).** [Rh(NH₃)₄chrysi]Cl₃ (**6**) (20 mg, 0.038 mmol) and **5a** (17.8 mg, 0.082 mmol, excess) were dissolved in a 1:1 mixture of ethanol and water (100 ml) and heated under reflux for 28 h. The solvent was removed *in vacuo*, and the crude product was purified by HPLC (95:5:0.001 H₂O:MeCN:TFA), using a C18 reverse-phase column (Varian, Inc). The purified product was dried under vacuum and redissolved in a minimal volume of water. The TFA counterion was exchanged for a chloride with a Sephadex QAE-125 ion-exchange resin primed with 1M MgCl₂. Yield: 4.5 mg (13.5%). ¹H NMR (DMSO-*d*₆, 300 MHz): δ 13.47 (s, 1H), 13.03 (s, 1H), 9.27 (d,



Scheme 2.2 Synthesis of $rac\text{-}[\text{Rh}(\text{L})_2\text{chrysi}]^{3+}$, where $\text{L} = 2\text{-}(\text{di}(\text{pyridine-2-yl})\text{amino})\text{ethanol}$ (DPAE, **5a**) or $\text{N-propyl-N-(pyridin-2-yl)pyridin-2-amine}$ (PrDPA, **5b**).

$J = 8.1$ Hz, 1H), 9.02-8.75 (overlapping m, 6H), 8.52-8.27 (overlapping m, 3H), 8.21-7.60 (overlapping m, 8H) 7.41-7.01 (m, 8H), 4.23-4.04 (m, 4H), 3.82 (s, 2H), 3.71-3.54 (m, 4H) ppm; UV-vis (H_2O pH 8): 297 nm ($47,000 \text{ M}^{-1} \text{ cm}^{-1}$), 391 nm ($9,300 \text{ M}^{-1} \text{ cm}^{-1}$). ESI-MS (cation): 787.1 m/z ($\text{M} - 2\text{H}^+$), 394.2 m/z ($\text{M} - \text{H}^{2+}$) obsd, 787 m/z ($\text{M} - 2\text{H}^+$) calcd.

2.2.3.3 *rac*-Rh(PrDPA)₂chrysi³⁺ (1b). **1b** was synthesized from **6** (20 mg, 0.038 mmol) and **5b** (17 mg, 0.08 mmol) as described for **1a**. The resulting product was purified by HPLC (95:5:0.001 H_2O :MeCN:TFA) and passed through a Sephadex QAE-125 ion-exchanged resin primed with 1M MgCl_2 to give the chloride salt. Yield: 3 mg (15%). ¹H NMR ($\text{DMSO-}d_6$, 300 MHz): δ 10.08 (d, $J = 8.6$ Hz, 1H), 8.05 (dd, $J = 26.7$, 8.6 Hz, 4H), 7.58 (dd, $J = 21.1$, 8.5 Hz, 4H), 7.46-7.32 (m, 6H), 7.27-7.11 (m, 3H), 6.90-6.78 (m, 8H), 0.97-0.85 (m, 4H), 0.62 (t, $J = 7.2$ Hz, 4H), 0.02 (t, $J = 7.3$ Hz, 6H) ppm; UV-vis: (H_2O pH 8): 295 nm ($51,000 \text{ M}^{-1} \text{ cm}^{-1}$), 388 nm ($13,000 \text{ M}^{-1} \text{ cm}^{-1}$). ESI-MS (cation): 783.1 m/z ($\text{M} - 2\text{H}^+$), 392.4 m/z ($\text{M} - \text{H}^{2+}$) obsd, 783 m/z calcd.

2.2.4 Octanol/Water Partition Coefficient (log P)

Solid $[\text{Rh}(\text{DPAE})_2\text{chrysi}]^{3+}$, $[\text{Rh}(\text{PrDPA})_2\text{chrysi}]^{3+}$, and $[\text{Rh}(\text{DIP})_2\text{chrysi}]^{3+}$ were dissolved in 10 ml 1-octanol-saturated H_2O . Aliquots (2 ml) of each sample were taken in triplicate, mixed with an equal volume of H_2O -saturated 1-octanol, and vortexed for 10 s. The samples were incubated at room temperature for 4 h and centrifuged for 5 min at 3000 rpm to allow for the separation of the two phases. The concentrations of rhodium in the aqueous and organic phases were determined by UV-vis; to account for the change in the molar absorptivity of rhodium in 1-octanol, $[\text{Rh}]_{\text{oct}}$ was defined as $[\text{Rh}]_{\text{stock}} - [\text{Rh}]_{\text{aq}}$. Log P is defined as $\log([\text{Rh}]_{\text{oct}}/[\text{Rh}]_{\text{aq}})$.

2.2.5 Cell Culture

HCT116N and HCT116O cells were grown in RPMI 1640 medium containing 10% FBS, 2 mM L- glutamine, 0.1 mM nonessential amino acids, 1 mM sodium pyruvate, 100 units/mL penicillin, 100 µg/mL streptomycin, and 400 µg/mL Geneticin (G418). Cells were grown in tissue culture flasks (Corning Costar, Acton, MA) at 37 °C and 5% CO₂ humidified atmosphere.

2.2.6 Cellular Proliferation ELISA

ELISAs were performed with HCT116N and HCT116O cells as described in the literature.²¹ Cells were incubated with varying concentrations of rhodium for the durations specified, then grown in rhodium-free media for the remainder of the 72 h period. After 48 h, BrdU was added, and at 72 h, BrdU incorporation was quantified by antibody assay.²¹ Cellular proliferation was expressed as a ratio of BrdU incorporation into treated cells versus that of untreated cells, and standard errors were calculated from five replicates.

2.2.7 Cellular Proliferation MTT

MTT experiments were performed with HCT116N and HCT116O cells as described in the literature.²² HCT116N and HCT116O cells were inoculated with rhodium and plated in 96-well plates at 50,000 cells/well. Cells were incubated for 24, 48, or 72h at 37 °C under humidified atmosphere. After the incubation period, MTT was added, and the cells were incubated for an additional 4 h. The resulting formazan crystals were solubilized over a period of 24 h at 37 °C, 5% CO₂. Formazan formation was quantified *via* electronic absorption at 550-600 nm with a reference wavelength of 690

nm. Cell viability is expressed as a function of formazan formation and normalized to that of untreated cells. Standard errors were calculated from five replicates.

2.2.8 Binding Competition Titrations

A 29-mer DNA hairpin containing a CC mismatch (*5'-GGCAGGCATG-GCTTTTGGCCATCCCTGCC-3') (underline denotes the mismatch; asterisk denotes the radiolabel) was labeled with ^{32}P at the 5'-end according to established procedures.²³ A 1:1 mixture of labeled and unlabeled DNA was prepared in buffer (100 mM NaCl, 20 mM NaP_i , pH 7.1) to a final concentration of 2 μM . The hairpin was annealed by heating to 90 $^\circ\text{C}$ for 10 min and slowly cooled to room temperature. To prepare samples for gel electrophoresis, 5 μL of a 4 μM solution of $[\text{Rh}(\text{bpy})_2\text{chrysi}]\text{Cl}_3$ (which photocleaves the DNA backbone at the site of a mismatch or abasic site upon irradiation⁸⁻¹⁰) and varying concentrations of non-photocleaving competitor complex (5 μL) were added to 2 μM annealed DNA hairpin (10 μL). A light control (10 μL DNA, 10 μL H_2O), a dark control (10 μL DNA, 5 μL $\text{Rh}(\text{bpy})_2\text{chrysi}^{3+}$, 5 μL Rh, no irradiation), and a positive control (10 μL DNA, 5 μL $\text{Rh}(\text{bpy})_2\text{chrysi}^{3+}$, 5 μL H_2O) were also prepared. Samples were vortexed and, except for the dark control, irradiated on an Oriel (Darmstadt, Germany) 1000-W Hg/Xe solar simulator (340-440 nm) for 15 min. Samples were then incubated at 37 $^\circ\text{C}$ for 20 min, dried, then electrophoresed through a 20 % denaturing polyacrylamide gel. The gel was exposed on a phosphor screen, phosphorimaged (See **Figure 2.2** for a representative autoradiogram), and the amounts of DNA cleavage were quantified using ImageQuant.

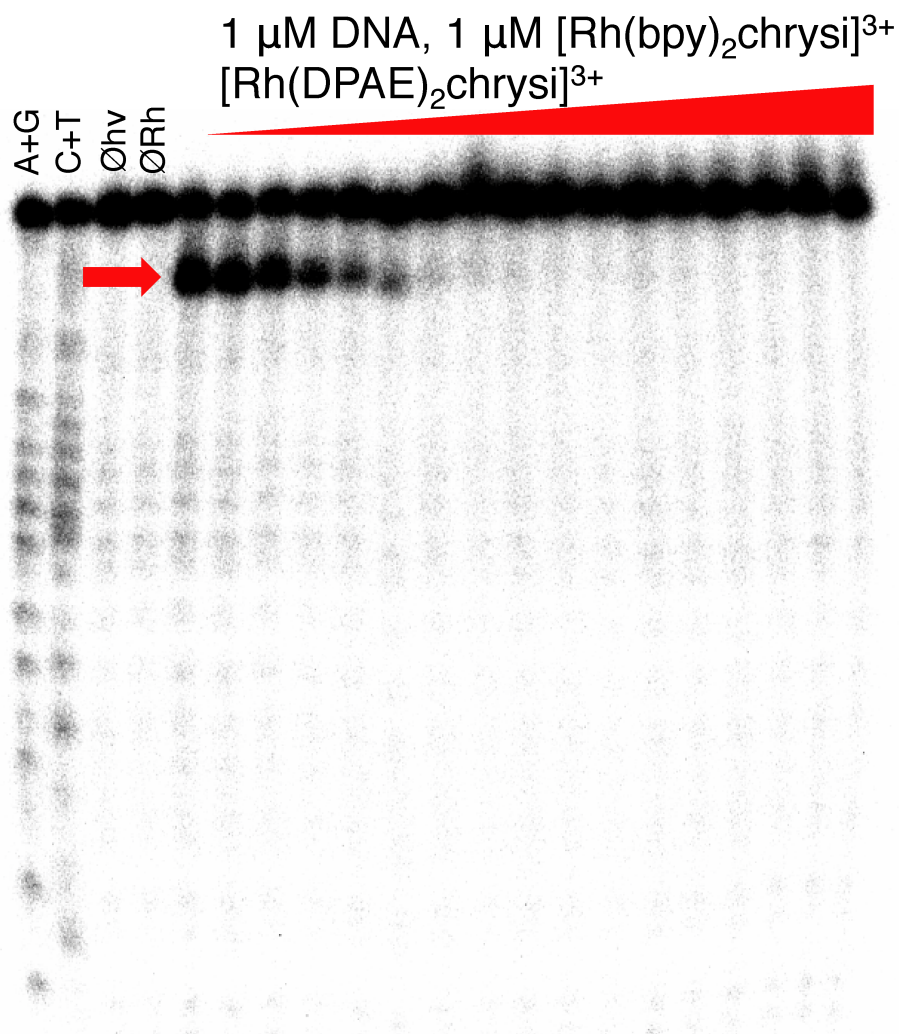


Figure 2.2 Binding affinities determined through DNA photocleavage. The DNA hairpin sequence is *5'-GGCAGGCATGGCTTTTTGCCATCCCTGCC-3' (underline denotes the mismatch, asterisk denotes the radiolabel). Samples were irradiated for 15 min and electrophoresed on a 20% denaturing PAGE gel. A light control (ØRh, without rhodium) and a dark control (Øhv, without irradiation) were included. A representative autoradiogram of a photocleavage competition titration between 1 μM *rac*- $[\text{Rh}(\text{bpy})_2\text{chrysi}]^{3+}$ and 0-50 μM $[\text{Rh}(\text{DPAE})_2\text{chrysi}]^{3+}$ is shown. Arrow indicates the position of the mismatch.

To determine the K_B values of each complex, competition gels were run in triplicate for each complex, and the percent DNA cleavage at each concentration was averaged and plotted as a function of $\log [Rh]$. The data were fitted to a sigmoidal curve using OriginPro 8.1. K_B values were determined by calculating the concentration of rhodium at the inflection points of the curve and solving simultaneous equilibria involving DNA, $Rh(bpy)_2chrysi^{3+}$, and the competitor complex in Mathematica 8.0. The dissociation constant K_D is defined as $1/K_B$.

2.2.9 Whole-Cell Rhodium Accumulation

HCT116O cells were plated in 6-well plates at 1.0×10^6 cells/well (3 ml media), and allowed 24 h to adhere. The cells were then incubated with 10 μM rhodium (except for $[Rh(DIP)_2chrysi]^{3+}$, which was administered at 2 μM) for a periods of 1, 3, 6, 12, or 24 h. Cells were lysed with 1% SDS and sonicated Qsonica Ultrasonic processor for 10 sec at 20% amplitude. Samples were aliquoted (0.8 ml) and diluted with 2% HNO_3 (0.8 ml), and cellular rhodium content was quantified on an HP-4500 ICP-MS unit. The remainder of the cell lysates were analyzed for protein content via bicinchoninic acid (BCA) assay.²⁴ Rhodium counts were normalized to cellular protein content, and standard errors were calculated from three replicates.

2.2.10 Mitochondrial Rhodium Accumulation

HCT116O cells were plated in 75 cm^2 culture flasks at 2.0×10^7 cells/plate and incubated at 37 $^\circ C$, 5% CO_2 for 24 h. Rhodium was added to 10 μM (except for $[Rh(DIP)_2chrysi]^{3+}$, which was administered at 2 μM) and cells were grown for an additional 24 h. The cells were then harvested by trypsinization and centrifuged for 5 min at 1,200 rpm. The supernatants were decanted, and the cell pellets were resuspended in 1

ml cold PBS (pH 7.2). The cells were centrifuged again for 5 min at 1,200 rpm. The supernatants were discarded, and the resultant pellets were resuspended in 0.5 ml mitochondrial extraction buffer (200 mM mannitol, 68 mM sucrose, 50 mM Pipes, 50 mM KCl, 5 mM EGTA, 2 mM MgCl₂; 1 mM DTT and protease inhibitors were added right before use). The samples were incubated on ice for 20 min, and the suspensions were homogenized via passage through a needle and syringe (35x). The homogenized cells were then centrifuged for 5 min at 750 rpm. The supernatants were collected and spun again at 14,000 g for 10 min. The supernatants were decanted, and the resulting mitochondrial pellet was suspended in 0.8 ml H₂O via probe sonication. All samples were diluted 1x with 2% HNO₃. Aliquots (20 uL) were used in a BCA assay to determine mitochondrial protein content, which was carried out according to standard protocol. Rh counts from ICP MS were converted to ppb and normalized to mitochondrial protein content (ng Rh/mg protein). As the mitochondria were isolated from whole cells, the rhodium content is strictly mitochondrial and therefore cannot be directly compared to total cellular rhodium accumulation. It should be noted that the Rh counts obtained are a lower-bound estimate, given the possibility of rhodium diffusion during organelle isolation. However, the experiments were performed in triplicate and were repeated by different experimenters at different times, and the results are comparable. The purity of mitochondrial fractions was ascertained by Western blot.²⁵

2.2.11 Nuclear Rhodium Accumulation

HCT1160 cells were plated in 75 cm² culture flasks at 1.5 x 10⁷ cells/plate and incubated at 37 °C , 5% CO₂, for 24 h. Rhodium was then added to 10 uM (except for [Rh(DIP)₂chrysi]³⁺, which was administered at 2 μM) and cells were grown for an

additional 24 h. The cells were trypsinized according to standard protocol, and the cell pellets were washed with 3 mL 1x PBS (pH 7.2) and spun at 1200 rpm for 5 min. The supernatant was discarded, and the pellets were resuspended in 1 mL 1x PBS and divided into 2 x 0.5 mL aliquots (nuclear and whole cell). The samples were spun at 450 g for 5 minutes at 4 °C. The supernatants were decanted and the whole cell pellets were dissolved in 1 mL Milli-Q water. The nuclear pellets were dissolved in 1 mL hypotonic buffer (20 mM Tris-HCl, pH 7.4; 10 mM NaCl, 3 mM MgCl₂) and incubated on ice for 15 min. After 15 min, 50 uL of NP-40 detergent were added and the samples were vortexed for 10 s. Samples were then spun at 3000 g for 10 min at 4 °C. The supernatants were discarded, and the nuclear pellets were dissolved in 1 mL Milli-Q water *via* sonication. All samples were diluted 1x with 2% HNO₃. 20 uL aliquots were used in a BCA assay to determine nuclear protein content, which was carried out according to standard protocol. Rh counts from ICP MS were converted to ppb and normalized to nuclear protein content (ng Rh/mg protein). Experiments were performed in biological triplicate, and standard errors were calculated from 6 replicates.

2.3 Results

2.3.1 Synthesis and Characterization of [Rh(DPAE)₂chrysi]³⁺ and [Rh(PrDPA)₂chrysi]³⁺

The complexes studied were prepared in a straightforward manner. The ancillary ligands, 2-(di(pyridin-2-yl)amino)ethanol (DPAE, **5a**) and *N*-propyl-*N*-(pyridin-2-yl)pyridin-2-amine (PrDPA, **5b**), were synthesized from 2,2'-dipyridylamine,²⁰ and the rhodium precursor, [Rh(NH₃)₄chrysi]³⁺ (**6**), is synthesized from [Rh(NH₃)₅Cl]²⁺.¹⁶ The *rac*-tris(chelate) complexes (**1a**, **1b**) are prepared by reacting **6** with either **5a** or **5b** (2.1

equiv) in a 1:1 mixture of ethanol and water at reflux temperature (Scheme 2). The octanol/water partition coefficients ($\log P$) were determined to be -1.5 and -1.0 for $[\text{Rh}(\text{DPAE})_2\text{chrysi}]^{3+}$ and $[\text{Rh}(\text{PrDPA})_2\text{chrysi}]^{3+}$, respectively, illustrating that simple functional group manipulations can appreciably alter the lipophilicity of a complex. These $\log P$ values for $[\text{Rh}(\text{DPAE})_2\text{chrysi}]^{3+}$ and $[\text{Rh}(\text{PrDPA})_2\text{chrysi}]^{3+}$ may be compared to that of $[\text{Rh}(\text{DIP})_2\text{chrysi}]^{3+}$, a highly lipophilic complex ($\log P = 1.3$) but with no cell-selective activity, given its poor binding to mismatches.

2.3.2 DNA Binding Affinity

Previously, a correlation between DNA binding affinity and inhibitory effects on MMR-deficient cells was established.¹⁶ In general, complexes that bind DNA mismatches with the highest affinity were found to have the greatest differential activity *in cellulose*, with the most effective complexes showing $K_B = 10^7 - 10^8 \text{ M}^{-1}$ for a CC mismatch. We thus sought to examine whether a difference in binding affinity might account for the differences seen in biological activities.

Since $[\text{Rh}(\text{DPAE})_2\text{chrysi}]^{3+}$ and $[\text{Rh}(\text{PrDPA})_2\text{chrysi}]^{3+}$ do not promote DNA photocleavage, DNA binding affinities were measured on a 29mer hairpin sequence – 5'-GGCAGGCATGGCTTTTTGCCATCCCTGCC-3' (underline denotes the mismatch) – containing a CC mismatch in a competition assay through photocleavage by $[\text{Rh}(\text{bpy})_2\text{chrysi}]^{3+}$.²³ For a CC mismatch, we find $K_B = 6.8 \times 10^6 \text{ M}^{-1}$ and $2.5 \times 10^6 \text{ M}^{-1}$ for $[\text{Rh}(\text{DPAE})_2\text{chrysi}]^{3+}$ and $[\text{Rh}(\text{PrDPA})_2\text{chrysi}]^{3+}$, respectively (see **Figure 2.3**). The binding affinity of $[\text{Rh}(\text{DPAE})_2\text{chrysi}]^{3+}$ for a CC-mismatch is therefore only slightly greater than that of $[\text{Rh}(\text{PrDPA})_2\text{chrysi}]^{3+}$. Both complexes show affinities well within the range where differential effects on biological activities have been seen.¹⁶ Thus,

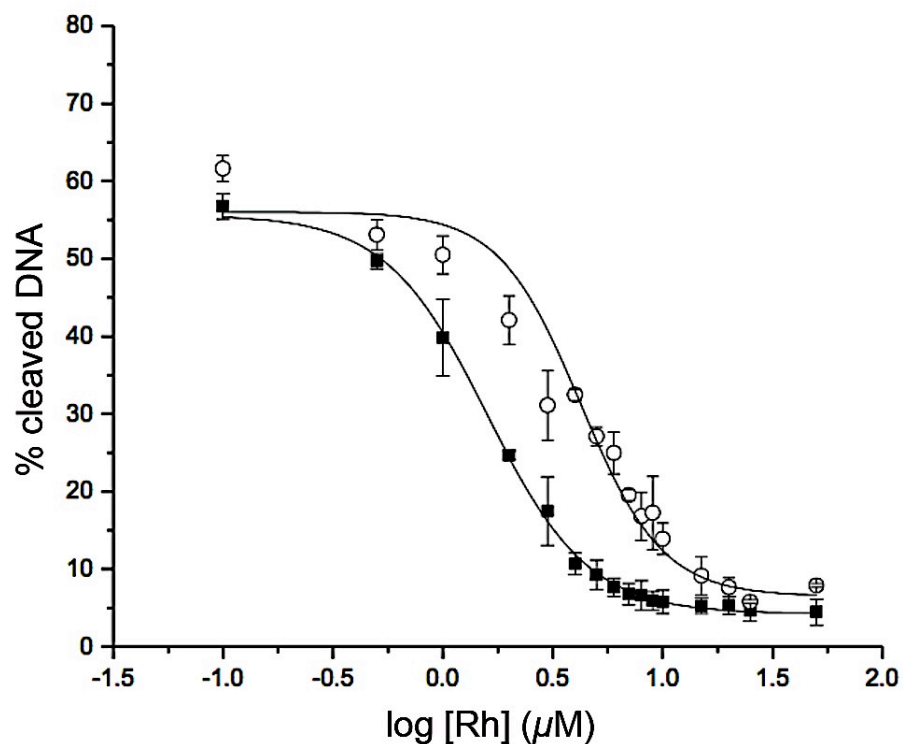


Figure 2.3 Sigmoidal curves (Boltzmann fit) for competition titrations with $\text{Rh}(\text{DPAE})_2\text{chrysi}^{3+}$ (■) and $\text{Rh}(\text{PrDPA})_2\text{chrysi}^{3+}$ (○). K_B was calculated by solving simultaneous equilibria at the inflection point of each curve. Experiments were conducted in buffer (50 mM NaCl, 10 mM NaPi, pH 7.1) using 1 μM DNA and 1 μM *rac*- $\text{Rh}(\text{bpy})_2\text{chrysi}^{3+}$, with 0-50 μM *rac*- $[\text{Rh}(\text{DPAE})_2\text{chrysi}]^{3+}$ or *rac*- $[\text{Rh}(\text{PrDPA})_2\text{chrysi}]^{3+}$ competitor complex. Error bars are calculated from three independent experiments performed for each complex.

binding affinity alone cannot account for the difference in biological activity between the two complexes.

The DNA binding affinities for all metalloinsertors in this study were determined in a similar manner. The results, along with those of all previously reported compounds,^{16,19} are shown in **Figure 2.4**. Interestingly, despite the variance in both the ancillary ligands and number of hydrogen-bond donors, all compounds (except the extremely bulky $[\text{Rh}(\text{DIP})_2(\text{chrysi})]^{3+}$) exhibit binding affinities within essentially the same order of magnitude, varying from $2.3 \times 10^6 \text{ M}^{-1}$ to $4.4 \times 10^7 \text{ M}^{-1}$.

2.3.3 Cellular Proliferation ELISA

We first tested for the selective effects on cellular proliferation of *rac*- $[\text{Rh}(\text{DPAE})_2\text{chrysi}]^{3+}$ and *rac*- $[\text{Rh}(\text{PrDPA})_2\text{chrysi}]^{3+}$ using the ELISA assay in the isogenic HCT116 cell lines testing for BrdU incorporation.²¹ HCT116N and HCT116O cells were incubated with varying concentrations of each complex, and the proliferation of each cell line was measured over time as a function of incorporation of the thymidine analog BrdU.²¹ The differential activity of rhodium treatment is defined as the difference between the normalized percentages of BrdU incorporation for the two cell lines.

As shown in **Figure 2.5**, $[\text{Rh}(\text{DPAE})_2\text{chrysi}]^{3+}$ exhibits differential inhibition of growth in the MMR-deficient cell line as early as 6 h. This activity is quite high and early compared to metalloinsertors tested in previous studies.¹⁶ By contrast, and remarkably, $[\text{Rh}(\text{PrDPA})_2\text{chrysi}]^{3+}$ displays little detectable selectivity for MMR-deficient cells; no activity is seen at 6 or 12 h. After 24 h of treatment with $[\text{Rh}(\text{PrDPA})_2\text{chrysi}]^{3+}$, inhibition of growth is observed in both cell lines, with little difference between them.

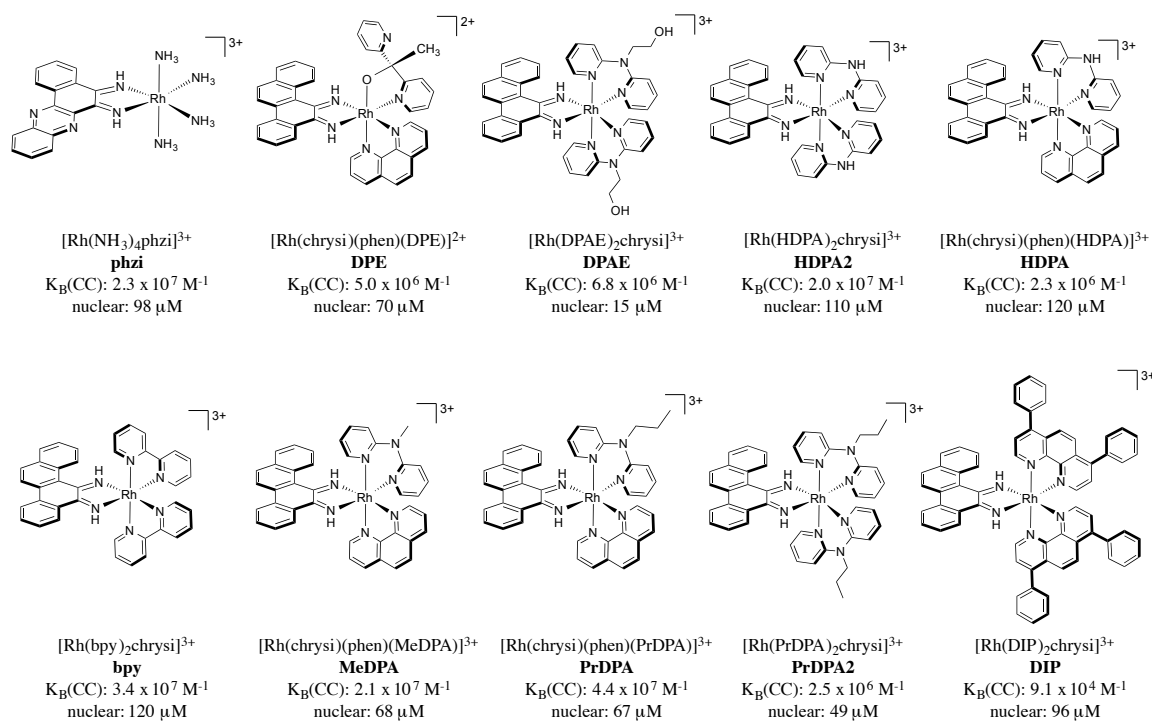


Figure 2.4 Chemical structures, binding affinities for CC mismatches, and

approximated nuclear concentration of all compounds studied. Binding affinities for $[Rh(DIP)_2(chrysi)]^{3+}$, $[Rh(HDPA)_2(chrysi)]^{3+}$, and $[Rh(bpy)_2(chrysi)]^{3+}$ are previously reported.^{10,16} All other compounds' DNA binding affinities were measured on the 29mer hairpin 5'-GGCAGGCATGGCTTTTGCCATCCCTGCC-3' (underline denotes the mismatch) in a competition assay through photocleavage by $[Rh(bpy)_2(chrysi)]^{3+}$. To determine nuclear rhodium concentrations, HCT116O cells were incubated in media containing 10 μM of each rhodium complex (except $[Rh(DIP)_2(chrysi)]^{3+}$, which was administered at 2 μM) for 24 h. The cells were harvested by trypsinization and the nuclei isolated. Rhodium content was quantified by ICP-MS first normalized to number of nuclei, then divided by the volume of the nucleus of a HCT116O cell, which was approximated as a sphere with radius 8 μm .³¹

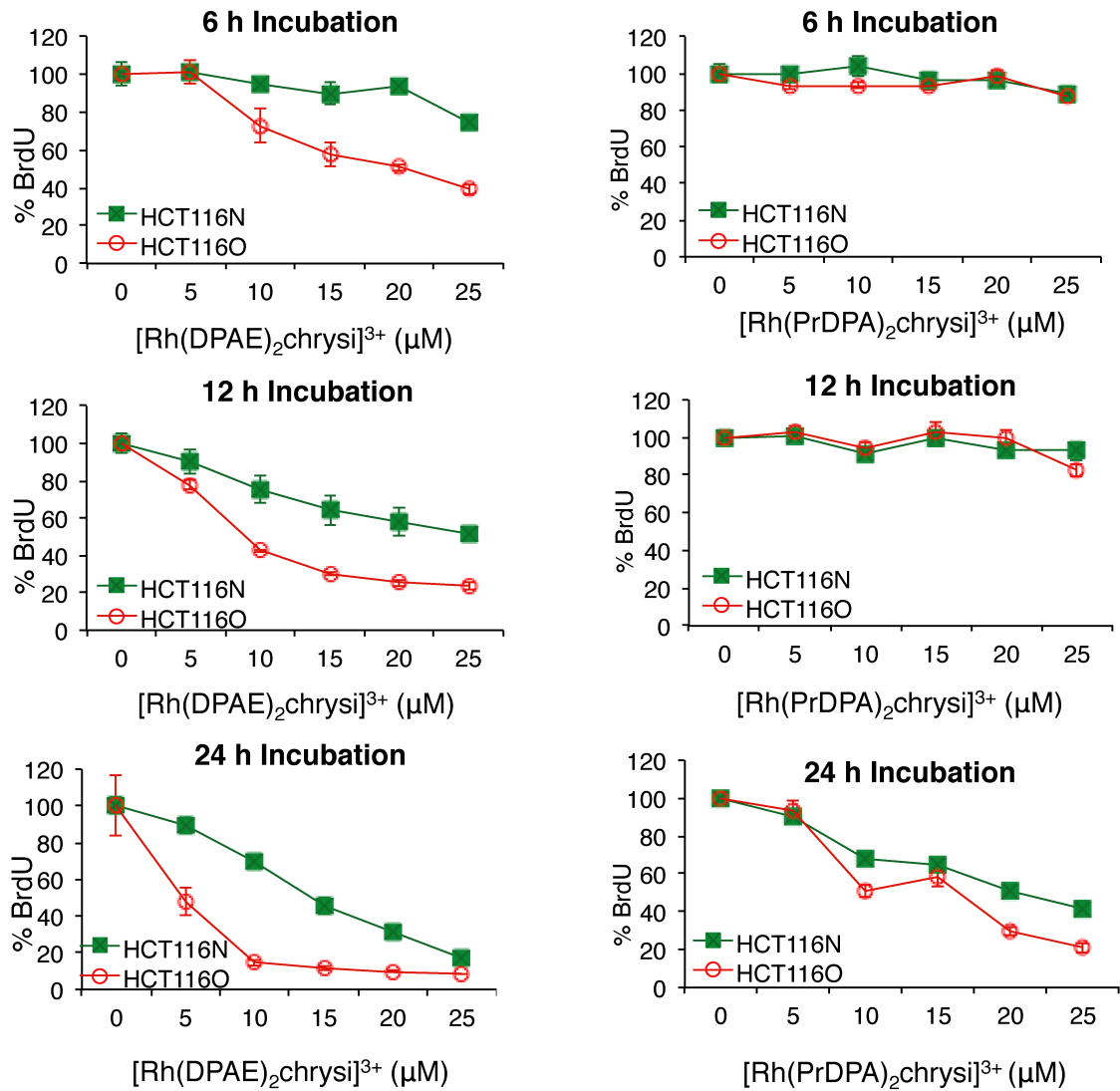


Figure 2.5 Inhibitory effects of $[\text{Rh}(\text{DPAE})_2\text{chrysi}]^{3+}$ (left) and $[\text{Rh}(\text{PrDPA})_2\text{chrysi}]^{3+}$ (right) as a function of incubation time on cellular proliferation in the MMR-proficient HCT116N (green) and MMR-deficient HCT116O (red) cell lines. Shown are plots of BrdU incorporation (a measure of DNA synthesis and therefore cellular proliferation) normalized to the BrdU incorporation of untreated cells as a function of rhodium concentration. Standard error bars for five trials are shown.

The biological effects of $[\text{Rh}(\text{DPAE})_2\text{chrysi}]^{3+}$ and $[\text{Rh}(\text{PrDPA})_2\text{chrysi}]^{3+}$ in MMR-proficient and MMR-deficient cells are representative of a larger trend observed among metalloinsertors. **Figure 2.6** summarizes the inhibitory effects, as determined by the ELISA, for all ten compounds at 10 μM rhodium concentration and 24 h of incubation (except $[\text{Rh}(\text{DIP})_2(\text{chrysi})]^{3+}$, which is shown at 2 μM), as these are the same conditions used for all ICP-MS experiments. There are four compounds with high selectivity for the MMR-deficient HCT116O cells ($[\text{Rh}(\text{NH}_3)_4(\text{phzi})]^{3+}$, $[\text{Rh}(\text{chrysi})(\text{phen})(\text{DPE})]^{3+}$, $[\text{Rh}(\text{DPAE})_2(\text{chrysi})]^{3+}$, and $[\text{Rh}(\text{HDPA})_2(\text{chrysi})]^{3+}$, all shown in different shades of blue), displaying differential inhibitions of $63 \pm 5\%$, $55 \pm 3\%$, $55 \pm 3\%$, and $52 \pm 2\%$, respectively. $[\text{Rh}(\text{chrysi})(\text{phen})(\text{HDPA})]^{3+}$ and $[\text{Rh}(\text{bpy})_2(\text{chrysi})]^{3+}$ exhibit modest selectivity with differential inhibitions of $27 \pm 2\%$ and $8 \pm 2\%$ at 24 h (shown in green in **Figure 2.6**). It should be noted that at longer incubation times the differential inhibition of $[\text{Rh}(\text{bpy})_2(\text{chrysi})]^{3+}$ increases.^{xx} $[\text{Rh}(\text{chrysi})(\text{phen})(\text{MeDPA})]^{3+}$, also shown in green, exhibits delayed biological activity. At 24 h incubation times, this complex does not display significant inhibition of DNA synthesis toward either cell line. The remaining compounds ($[\text{Rh}(\text{chrysi})(\text{phen})(\text{PrDPA})]^{3+}$, $[\text{Rh}(\text{PrDPA})_2(\text{chrysi})]^{3+}$, and $[\text{Rh}(\text{DIP})_2(\text{chrysi})]^{3+}$, shown in red) exhibit no selectivity for the MMR-deficient HCT116O cell line, and inhibit DNA synthesis similarly in both cell lines. It should be noted that none of the complexes studied show a differential inhibition favoring the HCT116N cell line, although that is the common result for many DNA damaging agents.

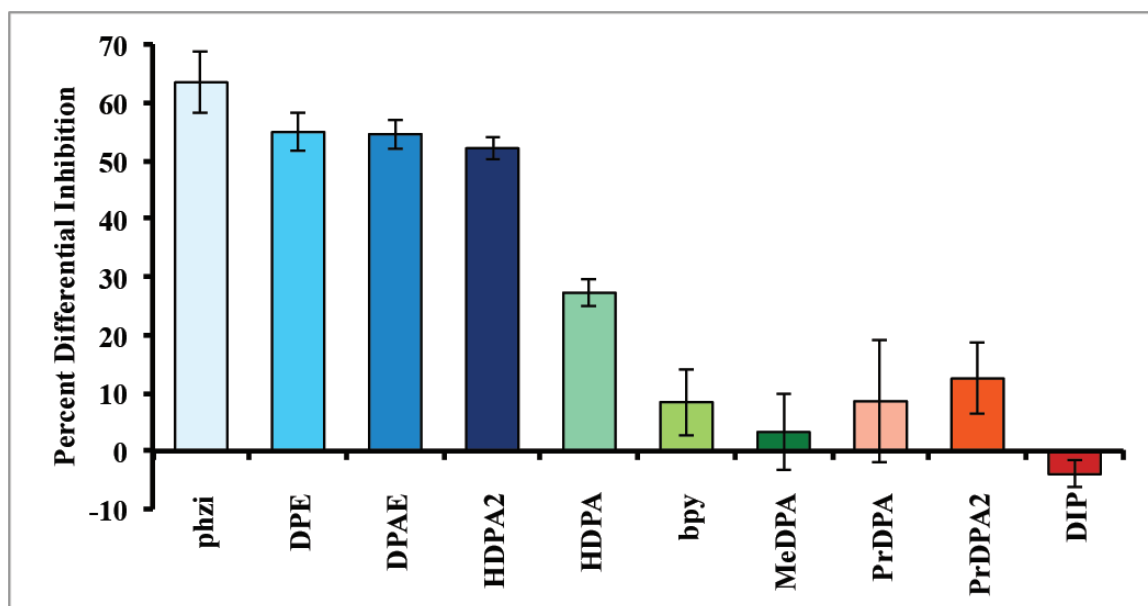


Figure 2.6 Inhibitory effects of rhodium metalloinsertors as a function of metalloinsertor identity. The percent differential inhibition is defined as the difference of the normalized percentages of cellular proliferation between the two cell lines, HCT116O versus HCT116N. ELISA analyses were performed as in **Figure 2.5**. Cells were incubated with 10 μM rhodium complex for 24 h (except $[\text{Rh}(\text{DIP})_2(\text{chrysi})]^{3+}$, which was administered at 2 μM).

2.3.4 MTT Cytotoxicity Assay

We next assayed for cytotoxicity using the MTT assay for mitochondrial function. Mitochondrial enzymes in metabolically active cells reduce 3-(4,5-dimethylthiazol-2-yl)-2,5-diphenyltetrazolium bromide (MTT), a yellow tetrazole to purple formazan, which can be quantified by its characteristic absorbance at 570 nm.²² As a result, viable cells appear deep purple, while dead cells remain yellow. The absorbance is typically an indicator of the percentage of viable cells present in the medium; however, it more directly reflects the metabolic activity of the cells, and specifically mitochondrion function.²⁶⁻²⁸ HCT116N and HCT116O cells were treated with varying concentrations of rhodium and incubated for 24, 48, or 72 h, after which the cells were exposed to MTT reagent for 4 h. The resulting formazan crystals were solubilized in acidified SDS and quantified using electronic absorption spectroscopy. The percentage of viable cells in a given sample is expressed as a function of the absorbance of formazan at 570 nm. We were interested in particular in comparing the two matched rhodium complexes – $[\text{Rh}(\text{DPAE})_2\text{chrysi}]^{3+}$ and $[\text{Rh}(\text{PrDPA})_2\text{chrysi}]^{3+}$ – directly. Neither showed significant differential effects in cytotoxicity at 24h. However, while we observe that cells treated with $[\text{Rh}(\text{DPAE})_2\text{chrysi}]^{3+}$ exhibit little cytotoxic effect at 24 h (**Figure 2.7**), cells treated with $[\text{Rh}(\text{PrDPA})_2\text{chrysi}]^{3+}$, show some loss in viability; for cells incubated with $[\text{Rh}(\text{PrDPA})_2\text{chrysi}]^{3+}$, the percentage of viable cells begins to decrease by 24 h, indicative of a change in metabolic activity. This effect for $[\text{Rh}(\text{PrDPA})_2\text{chrysi}]^{3+}$, however, is not found to be cell-selective.

With longer incubation periods, a selective cytotoxic effect is observed with $[\text{Rh}(\text{DPAE})_2\text{chrysi}]^{3+}$ in the MTT assay. After 48h incubation, $[\text{Rh}(\text{DPAE})_2\text{chrysi}]^{3+}$

exhibits a differential cytotoxicity of $41 \pm 5\%$ at its optimal concentration ($25 \mu\text{M}$), while $[\text{Rh}(\text{PrDPA})_2\text{chrysi}]^{3+}$ effects cytotoxicity in both cell lines equally (**Figure 2.8**). These

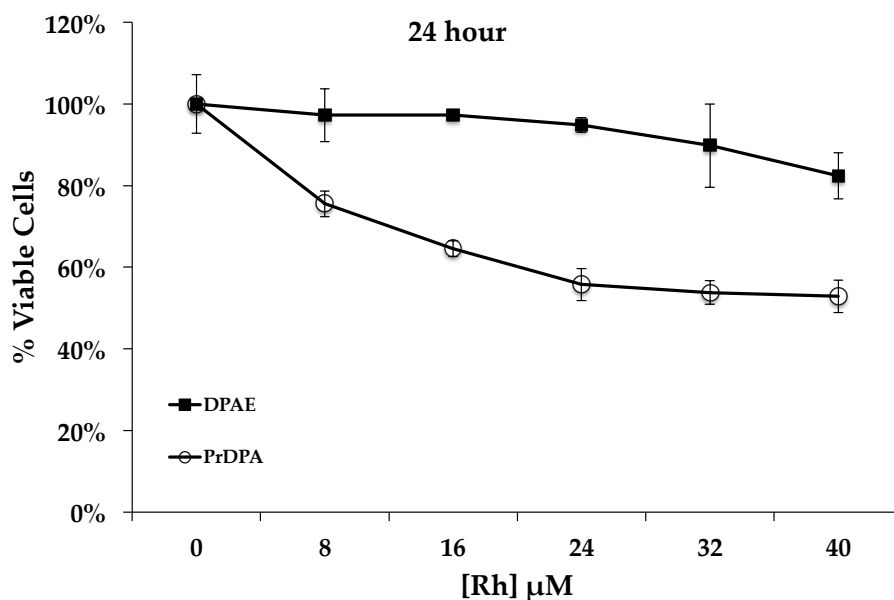


Figure 2.7 Cell viability of HCT116O cells treated with either $[\text{Rh}(\text{DPAE})_2\text{chrysi}]^{3+}$ (■) or $[\text{Rh}(\text{PrDPA})_2\text{chrysi}]^{3+}$ (●) over a 24 h period, as determined by MTT assay. Cells were plated in a 96-well format at densities of 5×10^4 cells/well and treated with the concentrations of rhodium metalloidinsertors indicated. After 24h, cells were labeled with MTT for 4h. The percentage of cell viability is normalized to that of untreated cells. The experiment was also performed with HCT116N cells, with similar results, as no differential cytotoxicity is observed with either complex at 24h. Standard error bars for five trials are shown.

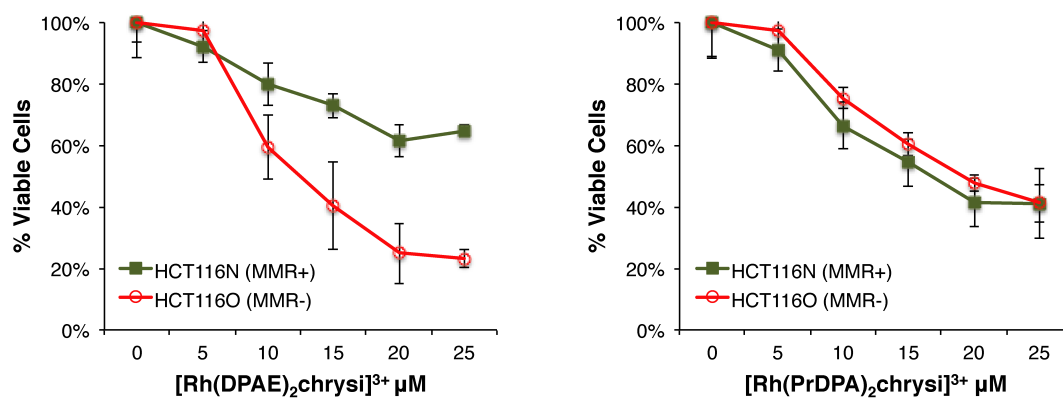


Figure 2.8 Differential cytotoxicities of rhodium metalloinsertors $[\text{Rh}(\text{DPAE})_2\text{chrysi}]^{3+}$ (left) and $[\text{Rh}(\text{PrDPA})_2\text{chrysi}]^{3+}$ (right). HCT116N (green) and HCT116O (red) cells were plated in 96-well format at densities of 5×10^4 cells/well and treated with the concentrations of rhodium metalloinsertors indicated. After 48 hours, the cells were labeled with MTT for 4 hours. The percentage of cell viability is normalized to that of untreated cells. Standard error bars for five trials are shown. The experiment was also performed with a 72h incubation period, with similar results (data not shown), and reflects the trends observed for all ten metalloinsertors with respect to the effects of lipophilicity on cell-selective biological activity.¹⁹

results are consistent with the activities of each complex in the ELISA and with the overall trends observed for all ten metalloinsertor complexes.¹⁹

2.3.5 Cellular Uptake of Metal Complexes

We explored the accumulation of rhodium in whole-cell extracts using inductively coupled plasma mass spectrometry (ICP-MS). Could the difference in biological function be explained through a difference in cellular uptake? To determine whole-cell uptake, HCT116O cells were incubated in media containing 10 μM rhodium for 24 h. Cells were rinsed with phosphate-buffered saline (PBS, pH 7.2) and lysed in a 1% SDS solution. Rhodium content was quantified using ICP-MS and normalized to cellular protein content as determined by a bicinchoninic acid (BCA) assay.²⁴

As is evident in **Figure 2.9**, it is apparent that it is $[\text{Rh}(\text{PrDPA})_2\text{chrysi}]^{3+}$ that is more efficiently taken up inside cells. $[\text{Rh}(\text{PrDPA})_2\text{chrysi}]^{3+}$ exhibits significantly more cellular rhodium accumulation than $[\text{Rh}(\text{DPAE})_2\text{chrysi}]^{3+}$ – about a four-fold increase. The whole-cell uptake of $[\text{Rh}(\text{PrDPA})_2\text{chrysi}]^{3+}$ after 24h was measured to be 705 ± 140 ng Rh/mg cellular protein, whereas accumulation of $[\text{Rh}(\text{DPAE})_2\text{chrysi}]^{3+}$ at 24h was determined to be 165 ± 65 ng Rh/mg cellular protein. HCT116N cells were treated similarly, and the same trends in uptake and localization were observed for both cell lines. The increased lipophilicity of $[\text{Rh}(\text{PrDPA})_2\text{chrysi}]^{3+}$ afforded by the alkyl moieties likely contributes to this enhanced cellular accumulation. Based upon cellular accumulation, then, $[\text{Rh}(\text{PrDPA})_2\text{chrysi}]^{3+}$ might be expected to show greater biological efficacy, contrasting what we observe.

The cellular rhodium accumulation was studied further over several incubation periods for all complexes. HCT116O cells were treated with 10 μM of each rhodium

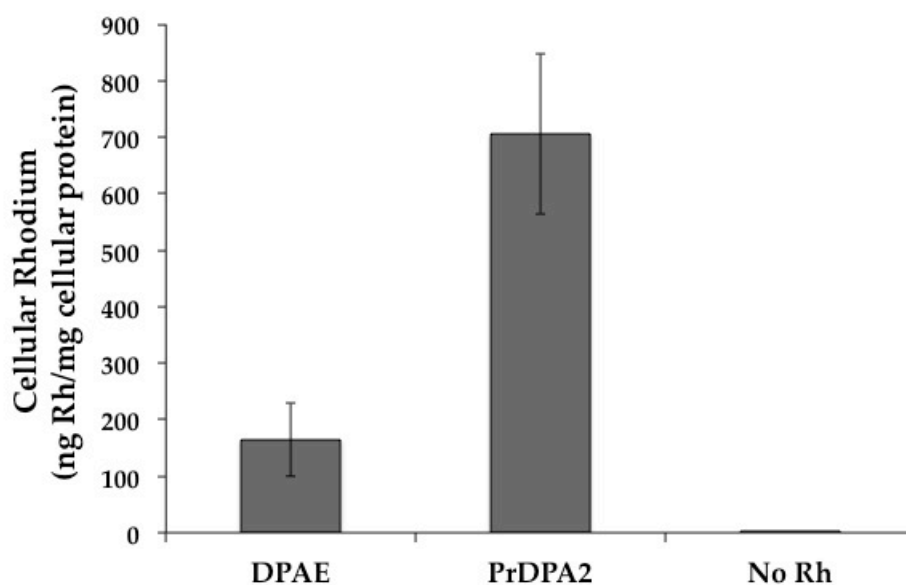


Figure 2.9 ICP-MS assay for rhodium uptake in whole cell extracts. HCT116O cells were incubated in media containing 10 μM of either $\text{Rh}(\text{DPAE})_2\text{chrysi}^{3+}$ (“DPAE”) or $\text{Rh}(\text{PrDPA})_2\text{chrysi}^{3+}$ (“PrDPA2”) for 24 h. Rhodium content was quantified by ICP-MS and normalized to cellular protein content, which was determined by BCA assay (See Section 2.2.9). $[\text{Rh}(\text{PrDPA})_2\text{chrysi}]^{3+}$ exhibits a four-fold greater uptake into the cell than $[\text{Rh}(\text{DPAE})_2\text{chrysi}]^{3+}$, a result of its increased lipophilicity.

complex (except $[\text{Rh}(\text{DIP})_2\text{chrysi}]^{3+}$, which was administered at 2 μM) for 1, 3, 6, 12, or 24 h. Whole cell lysates were analyzed for rhodium levels by ICP-MS and normalized to protein content as described above (**Figure 2.10**). The experiment was repeated with HCT116N cells to confirm that cellular uptake is not different for the HCT116O versus N cells and to verify consistency in trends among the ten complexes.

There seems to be a variety of different modes of uptake at play. The most lipophilic compounds, $[\text{Rh}(\text{chrysi})(\text{phen})(\text{PrDPA})]^{3+}$, $[\text{Rh}(\text{PrDPA})_2(\text{chrysi})]^{3+}$, and $[\text{Rh}(\text{DIP})_2(\text{chrysi})]^{3+}$, exhibit gradual uptake into the HCT116O cells, suggestive of passive diffusion. This is consistent with previous studies conducted on luminescent $[\text{Ru}(\text{L})_2\text{dppz}]^{2+}$ (dppz = dipyrido[3,2-a:2',3'-c]phenazine) analogues, demonstrating cellular accumulation through passive diffusion, facilitated by the negative potential difference across the cell membrane,^{29,30} The two compounds that exhibit delayed biological activity in the ELISA assay ($[\text{Rh}(\text{chrysi})(\text{phen})(\text{MeDPA})]^{3+}$ and $[\text{Rh}(\text{bpy})_2(\text{chrysi})]^{3+}$) exhibit no increase in cellular rhodium levels after initial uptake at 1 hour. Furthermore, the two compounds with HDPA ligands exhibit an enhanced cellular uptake despite reduced lipophilicities. They show a very high initial uptake, followed by a slight increase over the next 23 hours. The MeDPA compound does not exhibit the increase in uptake that we had expected, given its enhanced lipophilicity compared to the HDPA analog and likely pointing to a completely different mechanism of uptake. The two compounds with PrDPA ligands do exhibit enhanced uptakes compared to their respective HDPA analogs at 24 hr, but not nearly to the degree we would have expected based on lipophilicities. However, both the PrDPA compounds appear to be taken up through passive diffusion, unlike the HDPA compounds. Perhaps

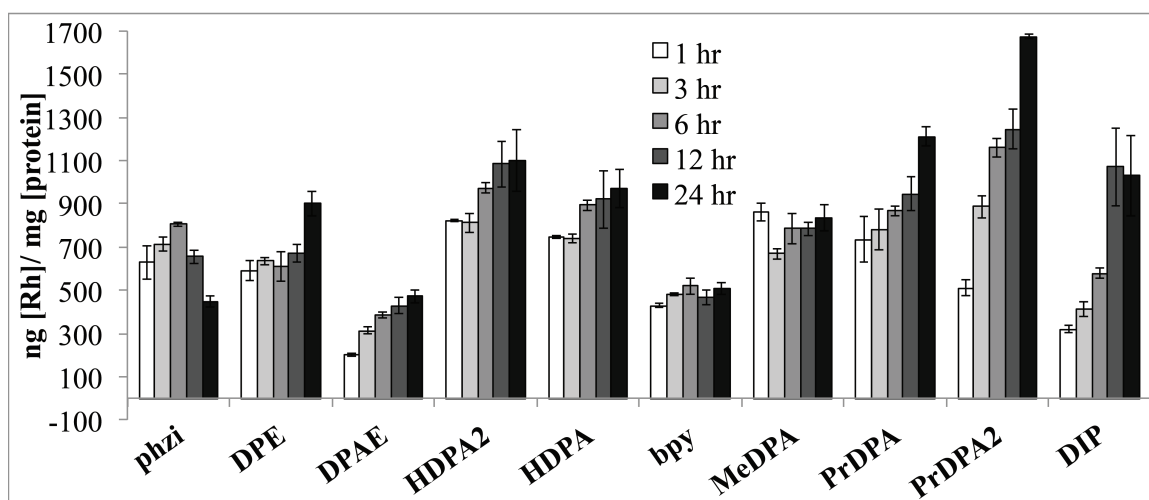


Figure 2.10 ICP-MS assay for whole-cell rhodium accumulation. HCT1160 cells were treated with 10 μM of each rhodium complex (except $[\text{Rh}(\text{DIP})_2(\text{chrysi})]^{3+}$, which was administered at 2 μM) for 1, 3, 6, 12, or 24 h. The cells were analyzed for rhodium content by ICP-MS. The rhodium counts were normalized to protein content, which was determined by a BCA assay. See Section 2.2.9.

the fact that the HDPA ligand has the potential to form hydrogen bonds *in cellulose* is important to its path into the cell. The compounds that exhibit the highest selectivities in the biological assays ($[\text{Rh}(\text{chrysi})(\text{phen})(\text{DPE})]^{3+}$, $[\text{Rh}(\text{DPAE})_2(\text{chrysi})]^{3+}$, and $[\text{Rh}(\text{NH}_3)_4(\text{phzi})]^{3+}$) by no means have the highest overall rhodium levels. In fact, all three of them have among the lowest amount of rhodium uptake into cells.

2.3.7 ICP-MS Assay for Nuclear Rhodium Levels

HCT116O cells were treated with 10 μM of each rhodium complex (except $[\text{Rh}(\text{DIP})_2(\text{chrysi})]^{3+}$, which was administered at 2 μM) for 24 h. The cells were harvested by trypsinization and the nuclei were isolated. Nuclear rhodium levels were determined by ICP-MS and normalized to protein content. The protein content was converted to number of nuclei by the conversion factors 3.28×10^{-8} mg [nuclear protein]/nuclei (found by counting cells or nuclei with a hemacytometer followed by lysing and protein quantification). The rhodium concentrations were then divided by nuclei density to obtain ng of rhodium per nucleus. The process was repeated with HCT116N cells to confirm that the two cell lines behave similarly and to verify consistency in trends among the ten compounds. These numbers can be used to estimate nuclear concentrations by approximating the nucleus of a HCT116O cell as a sphere with radius 4 μm .³¹ The approximate nuclear rhodium concentrations, so determined, are reported in **Figure 2.4**.

As can be seen in **Figure 2.11**, there is little correlation between cell-selective activity and nuclear rhodium concentration. In fact, all nuclear rhodium concentrations except for that of $[\text{Rh}(\text{DPAE})_2(\text{chrysi})]^{3+}$ are within a factor of 2 of each other and hardly vary among the 10 compounds. When we approximate the nuclear concentrations in molarity of the 10 compounds, all compounds are present in the nucleus at concentrations

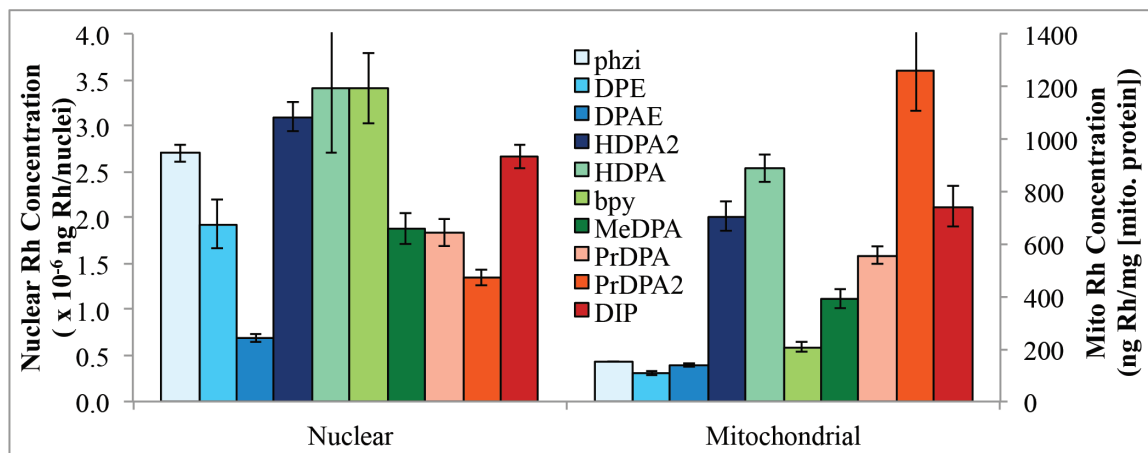


Figure 2.11 ICP-MS assay for nuclear and mitochondrial rhodium accumulation.

HCT1160 cells were treated with 10 μ M of each rhodium complex (except $[\text{Rh}(\text{DIP})_2(\text{chrysi})]^{3+}$, which was administered at 2 μ M) for 24 h. The cells were harvested by trypsinization and appropriate organelle isolation procedures performed. The mitochondrial rhodium counts were normalized to protein content, which was determined by a BCA assay. The nuclear rhodium numbers were normalized to number of nuclei.

on the order of 10^{-5} to 10^{-4} M. These concentrations are all more than 2 orders of magnitude higher than the binding affinities for *in vitro* mismatch detection (yet below non-specific DNA binding levels). Thus, even estimating the error on these numbers to be an order of magnitude, all compounds are present in the nucleus at concentrations sufficient for mismatch binding.

2.3.8 ICP-MS Assay for Mitochondrial Rhodium Levels

HCT1160 cells were treated with 10 μ M of each rhodium complex (except $[\text{Rh}(\text{DIP})_2(\text{chrysi})]^{3+}$, which was administered at 2 μ M) for 24 h. The cells were harvested by trypsinization, the mitochondria were isolated, and the rhodium levels were analyzed by ICP-MS and normalized to protein content. The results are summarized in **Figure 2.11** alongside the nuclear concentrations. The fact that the three compounds with the most cell-selective biological activity ($[\text{Rh}(\text{NH}_3)_4(\text{phzi})]^{3+}$, $[\text{Rh}(\text{chrysi})(\text{phen})(\text{DPE})]^{3+}$, and $[\text{Rh}(\text{DPAE})_2(\text{chrysi})]^{3+}$, shown in blue) have the lowest mitochondrial rhodium accumulation, 152 ± 3 ng [Rh]/ mg [mitochondrial protein], 106 ± 7 ng [Rh]/ mg [mitochondrial protein], and 141 ± 8 ng [Rh]/ mg [mitochondrial protein], respectively, is striking. This correlation indicates that the biological target of our rhodium metalloinsertors is genomic DNA rather than mitochondrial DNA.

Furthermore, the three compounds that exhibit no selectivity for the MMR-deficient HCT1160 cell line in both biological assays ($[\text{Rh}(\text{chrysi})(\text{phen})(\text{PrDPA})]^{3+}$, $[\text{Rh}(\text{PrDPA})_2(\text{chrysi})]^{3+}$, and $[\text{Rh}(\text{DIP})_2(\text{chrysi})]^{3+}$, shown in red) display the highest levels of mitochondrial rhodium accumulation, 560 ± 30 ng [Rh]/ mg [mitochondrial protein], 1260 ± 150 ng [Rh]/ mg [mitochondrial protein] and 740 ± 70 ng [Rh]/ mg [mitochondrial protein], respectively. This result points to mitochondrial targeting as

responsible for the promiscuous biological activity associated with these three compounds that detracts from the cell-selective activity. The two HDPA-containing compounds stray from the trends observed with the other eight compounds.

2.4 Discussion

2.4.1 Biological Activity of Rhodium Metalloinsertors

The compounds displayed in **Figure 2.1** and **Figure 2.4** were synthesized initially in order to investigate the biological effects of varying the lipophilicity of the metalloinsertor. Surprisingly, all compounds exhibited binding affinities within the same order of magnitude (except $[\text{Rh}(\text{DIP})_2(\text{chrysi})]^{3+}$, which was included in the study as a reference compound with extreme lipophilicity, poor binding to mismatches, and no selectivity in our biological assays). The differences among these nine compounds in the ELISA and MTT assays therefore arise from primarily biological effects rather than mismatch binding.

Two of these complexes in particular, $[\text{Rh}(\text{DPAE})_2\text{chrysi}]^{3+}$ and $[\text{Rh}(\text{PrDPA})_2\text{chrysi}]^{3+}$, most simply illustrate the sensitivity of these biological effects to the lipophilicity of the complex. These metalloinsertors are highly similar in structure and DNA binding affinity (displaying K_B values within a factor of 2 at a CC mismatch), but only the DPAE complex exhibits cell-selective targeting of MMR-deficient cells. It is remarkable that this biological effect depends so sensitively on the chemical structure of the ancillary ligands. Substitution of the terminal alcohols on the dipyridylamine ligands for methyl groups is sufficient to extinguish the differential inhibition of cellular proliferation. It is moreover neither mismatch binding nor whole cell uptake that is

responsible for this effect; the complexes show quite similar DNA binding affinities and, indeed, there is superior whole-cell uptake of $[\text{Rh}(\text{PrDPA})_2\text{chrysi}]^{3+}$.

For all compounds, the cytotoxic effects seen in the MTT assay reflect the antiproliferative activity seen in the ELISA. Both compounds that exhibit delayed activity in the ELISA, $[\text{Rh}(\text{chrysi})(\text{phen})(\text{MeDPA})]^{3+}$ and $[\text{Rh}(\text{bpy})_2(\text{chrysi})]^{3+}$, do not show any significant cytotoxicity in the MTT assay. Furthermore, the four compounds with the largest differential inhibitions in the ELISA assay, $[\text{Rh}(\text{NH}_3)_4(\text{phzi})]^{3+}$, $[\text{Rh}(\text{chrysi})(\text{phen})(\text{DPE})]^{3+}$, $[\text{Rh}(\text{DPAE})_2(\text{chrysi})]^{3+}$, and $[\text{Rh}(\text{HDPA})_2(\text{chrysi})]^{3+}$, also show the largest differential cytotoxicities by the MTT assay. Finally, the three compounds with no differential activity in the ELISA assay, $[\text{Rh}(\text{chrysi})(\text{phen})(\text{PrDPA})]^{3+}$, $[\text{Rh}(\text{PrDPA})_2(\text{chrysi})]^{3+}$, and $[\text{Rh}(\text{DIP})_2(\text{chrysi})]^{3+}$, also show no differential cytotoxicity in the MTT assay. It is important to distinguish the absence of differential activity, where the compound shows no selectivity for one cell line over the other and affects both cell lines to the same degree, versus the absence of all activity, where the compound shows no appreciable biological effect on either cell line.

Significantly, the biological activities of these compounds vary dramatically despite their similar binding affinities. Interestingly, the effect of appending a lipophilic alkyl chain to the back of the HDPA ligand either significantly slows down all activity, as with the MeDPA derivative, or instead abolishes the selectivity of the compound for the MMR-deficient HCT116O cell line, as with the PrDPA derivatives. While the mechanism of inhibition is not yet fully understood, one possible scenario is protein recognition of the metalloinsertor-mismatch complex, generating a covalent protein-DNA lesion. Bulky tethers off the back of the metalloinsertor may inhibit the formation of such

a lesion, leading to the aforementioned observations. Yet another explanation for the results might be that the increased lipophilicity of the metalloinsertor enhances uptake into the cell but also alters the subcellular localization of the complex once it has entered the cell. This altered subcellular localization could be the reason for the lack of selectivity of the compound for one cell line over the other. Indeed, the least lipophilic compounds have the most selective biological activity, while the more lipophilic compounds exhibit no selective biological activity.

2.4.2 Biological Effects of Simple Changes in Functionality on Rhodium Metalloinsertors

The analyses of subcellular rhodium accumulation in the nucleus and mitochondria have revealed significant structure-activity trends, primarily associated with ligand lipophilicity, across a family of ten metalloinsertor complexes. This structure activity relationship is illustrated most dramatically in the matched $[\text{Rh}(\text{DPAE})_2\text{chrysi}]^{3+}$ and $[\text{Rh}(\text{PrDPA})_2\text{chrysi}]^{3+}$ complexes. As illustrated in **Figure 2.12**, mitochondrial rhodium content in cells incubated with $[\text{Rh}(\text{PrDPA})_2\text{chrysi}]^{3+}$ exceeds that of cells grown in the presence of $[\text{Rh}(\text{DPAE})_2\text{chrysi}]^{3+}$ by nearly 10 fold. As with whole-cell uptake, the mitochondrial accumulation of $[\text{Rh}(\text{PrDPA})_2\text{chrysi}]^{3+}$ can likely be attributed to the lipophilic ancillary ligands, facilitating uptake of the lipophilic cation in response to mitochondrial membrane potential. It is understandable that this greater accumulation of $[\text{Rh}(\text{PrDPA})_2\text{chrysi}]^{3+}$ in mitochondria likely accounts for the MTT results.

Interestingly, while the more lipophilic $[\text{Rh}(\text{PrDPA})_2(\text{chrysi})]^{3+}$ complex has about a four-fold greater uptake into the cell than the polar $[\text{Rh}(\text{DPAE})_2(\text{chrysi})]^{3+}$ complex, it exhibits a ten-fold greater mitochondrial accumulation than the DPAE

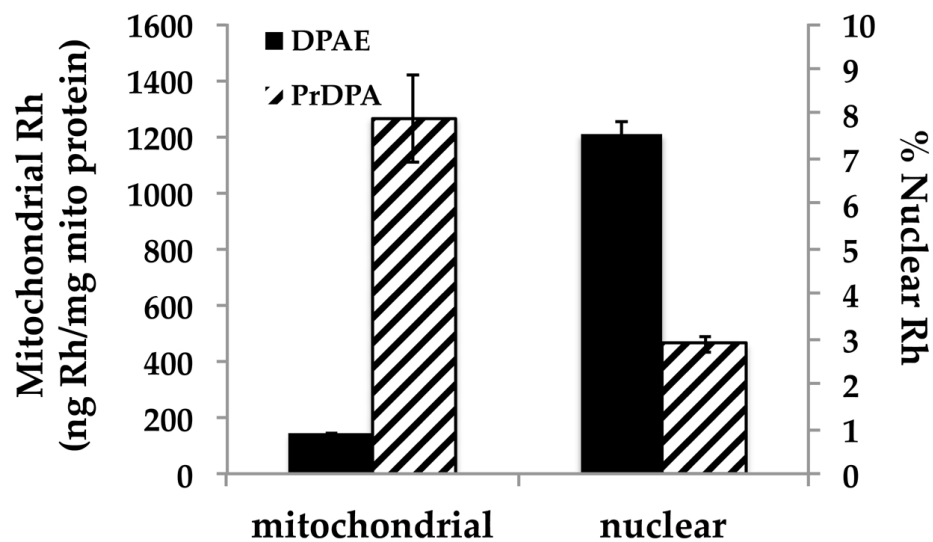


Figure 2.12 ICP-MS assay for rhodium uptake in nuclear and mitochondrial fractions. HCT1160 cells were incubated in media containing 10 μM of either $\text{Rh}(\text{DPAE})_2\text{chrysi}^{3+}$ (black) or $\text{Rh}(\text{PrDPA})_2\text{chrysi}^{3+}$ (hashed) for 24 h. The cells were harvested by trypsinization and appropriate organelle isolation procedures performed. The mitochondrial rhodium counts (left axis) were normalized to protein content, which was determined by a BCA assay. The nuclear rhodium numbers (right axis) were normalized to number of nuclei and expressed as a percentage of the total cellular rhodium.

complex, and only a two-fold greater nuclear concentration. However, the significantly increased cellular accumulation of $[\text{Rh}(\text{PrDPA})_2\text{chrysi}]^{3+}$ results in a higher proportion of rhodium in the cytosol and mitochondria, and it is here where cytotoxic effects that are not cell-selective must be triggered. By contrast, there is a comparatively smaller amount of extranuclear $[\text{Rh}(\text{DPAE})_2\text{chrysi}]^{3+}$, which by extension results in a lower mitochondrial concentration. Furthermore, as can be seen in **Figure 2.12**, a larger *percentage* of total cellular $[\text{Rh}(\text{DPAE})_2\text{chrysi}]^{3+}$ localizes in the nucleus, despite accruing in lower concentrations than the other complexes studied, including $[\text{Rh}(\text{PrDPA})_2\text{chrysi}]^{3+}$ (**Figures 2.4** and **2.11**). In the case of $[\text{Rh}(\text{PrDPA})_2\text{chrysi}]^{3+}$, in contrast, less than 3% of the total cellular rhodium resides in the nucleus. Clearly, it is nuclear trafficking, in conjunction with a lower fraction of extranuclear rhodium, that is responsible for the biological efficacy of $[\text{Rh}(\text{DPAE})_2\text{chrysi}]^{3+}$. Indeed, for $[\text{Rh}(\text{PrDPA})_2\text{chrysi}]^{3+}$, the nuclear rhodium content may largely reside in the membrane. For the DPAE complex, MMR-selective effects of the complex prevail over any nonspecific consequences of mitochondrial accumulation.

Perhaps most significantly, these data identify quite simply that metalloinsertors target mismatch lesions in genomic DNA rather than those in mitochondrial DNA. It is this nuclear mismatch targeting that is responsible for the differential biological activity in MMR-deficient cells that we observe.

2.4.3 Metalloinsertor Uptake and Nuclear Accumulation

The biological implications of ligand lipophilicity seen with $[\text{Rh}(\text{DPAE})_2\text{chrysi}]^{3+}$ and $[\text{Rh}(\text{PrDPA})_2\text{chrysi}]^{3+}$ are in fact general trends among metalloinsertor complexes. Table **2.1** displays qualitative nuclear and mitochondrial uptake properties, as well as the

Table 2.1 Qualitative nuclear^a and mitochondrial^b uptake properties, as well as the presence or absence of cell-selective biological activity^c for all ten metalloinsertors.

Compound	Nuclear Conc. ^a	Mito.Conc. ^b	Cell-Selective Activity ^c
[Rh(NH ₃) ₄ phzi] ³⁺	+	–	+
[Rh(chrysi)(phen)(DPE)] ²⁺	+	–	+
[Rh(DPAE) ₂ chrysi] ³⁺	+	–	+
[Rh(HDPA) ₂ chrysi] ³⁺	+	+	+
[Rh(chrysi)(phen)(HDPA)] ³⁺	+	+	+
[Rh(bpy) ₂ chrysi] ³⁺	+	+	–
[Rh(chrysi)(phen)(MeDPA)] ³⁺	+	+	–
[Rh(chrysi)(phen)(PrDPA)] ²⁺	+	+	–
[Rh(PrDPA) ₂ chrysi] ³⁺	+	+	–
[Rh(DIP) ₂ chrysi] ³⁺	+	+	–

^a Compound is considered to have “+” nuclear concentration if its nuclear concentration is sufficient for mismatch detection given its binding affinity. ^b Compound is considered to have “+” mitochondrial concentration if its mitochondrial rhodium concentration is ≥ 200 ng Rh/mg [mito protein]. ^c Compound is considered to have “+” cell-selective activity if its differential inhibition of DNA synthesis as measured by ELISA of the MMR-proficient line versus the MMR-deficient line is $\geq 25\%$ at 24h of incubation, 10 μ M compound concentration.

presence or absence of cell-selective biological activity for all ten metalloinsertors. Importantly, the biological effects seen in both assays can be explained by the subcellular localization of the metalloinsertors. If passive diffusion were the dominant mode of cellular uptake for these metalloinsertors,^{29,30} the more lipophilic compounds would be expected to have increased cellular uptake. And indeed, except for the HDPA compounds, the most lipophilic compounds do exhibit the greatest cellular accumulation. However, the more lipophilic compounds are in general associated with little differential biological activity; high accumulations of these metalloinsertors are toxic.

By altering L in $[\text{Rh}(\text{chrysi})(\text{phen})(\text{L})]^{3+}$ from HDPA to MeDPA to PrDPA, we do not observe an increase in uptake. In fact, the HDPA complex seems to show enhanced uptake in comparison with those that are more lipophilic. Furthermore, both compounds that possess HDPA ligands display both enhanced and accelerated uptake. This is likely due to additional uptake pathways facilitating the influx of complexes containing HDPA. Indeed, several bis(cyclometalated) iridium(III) polypyridine complexes have been shown to employ more than one mechanism of uptake,³² and this may be the case for several of our metalloinsertors. In comparing $[\text{Rh}(\text{PrDPA})_2(\text{chrysi})]^{3+}$ to $[\text{Rh}(\text{DPAE})_2(\text{chrysi})]^{3+}$, it appears that by altering the methyl group of PrDPA to an alcohol, uptake is decreased by a factor of four, yet only the DPAE compound has cell-selective activity. Lastly, the most polar compound, $[\text{Rh}(\text{NH}_3)_4(\text{phzi})]^{3+}$, displays a peak in uptake at 3 hours, after which cellular rhodium levels seem to decrease steadily. This is most likely caused by an efflux mechanism, that is, pumping the complex out of the cell. The ATP-binding cassette protein ABCG2 has been reported to be overexpressed in HCT116 cells,³³ is known to exhibit substrate promiscuity,³⁴ and may be responsible.

Contrary to what would be expected, three of the four compounds with the best activity have among the lowest cellular uptake at 24 hours, while the three compounds with no cell-selective activity have among the highest cellular uptake at 24 hours. It appears as though increased cellular uptake is actually detrimental to the unique cell-selective behavior of our metalloinsertors.

Significantly, the nuclear rhodium concentrations vary only slightly among the ten compounds. Importantly, by approximating the nucleus of an HCT116O cell as a sphere with diameter 8 μm ,³¹ all of our metalloinsertors are present in the nucleus at sufficient concentrations for mismatch binding, given their in vitro binding affinities (See **Figure 2.4**). Moreover, all metalloinsertors are below non-specific DNA binding concentrations, which precludes non-specific DNA binding as a possible cause of the non-selective toxicity seen with 3 of our metalloinsertors. The only difference between the two cell lines is the presence of a functional copy of the MLH1 gene in the HCT116N cell line, which encodes for a MMR protein found in the nucleus.³⁵ Therefore, any interactions the rhodium complexes have with the cell that are not associated with the nucleus may account for their nonspecific biological activity. Consequently, if nuclear DNA were the only cellular target for these metalloinsertors, then all compounds should exhibit similar differential activity due to their similar nuclear concentrations. However, these metalloinsertors could also interact with mitochondrial DNA, or become sequestered in lipid membranes throughout the cell (including the nuclear membrane, which would cause the nuclear rhodium concentration of such a complex to appear higher than it actually is), both of which would result in nonspecific biological activity.

2.4.4 Mitochondrial Accumulation of Rhodium Metalloinsertors

Importantly, the metalloinsertors that display highly cell-selective biological activity are generally associated with lower mitochondrial rhodium accumulation (**Figure 2.11**, complexes shown in blue), while the metalloinsertors that display non-selective toxicity show larger mitochondrial rhodium accumulation (**Figure 2.11**, complexes shown in red). These observations suggest that it is nuclear DNA targeting of our metalloinsertors that is responsible for their cell-selective biological activities rather than mitochondrial DNA targeting.

The two compounds $[\text{Rh}(\text{DPAE})_2(\text{chrysi})]^{3+}$ and $[\text{Rh}(\text{PrDPA})_2(\text{chrysi})]^{3+}$ exhibit this phenomenon quite simply. The only structural difference between the two compounds is the substitution of the methyl group of the PrDPA ligand for a primary alcohol in the DPAE ligand. While this substitution is structurally minute, the consequences of such a substitution are extreme from a biological standpoint. This substitution causes a large increase in polarity for the DPAE complex, as can be quantified by a decrease in the logP values from -1.0 to -1.5. Significantly, this increase in polarity is accompanied by an increase in cell-selective biological activity. While the more lipophilic $[\text{Rh}(\text{PrDPA})_2(\text{chrysi})]^{3+}$ complex exhibits no selectivity for the MMR-deficient cell line, the more polar $[\text{Rh}(\text{DPAE})_2(\text{chrysi})]^{3+}$ complex is highly selective for the MMR-deficient line over the MMR-proficient line. Furthermore, this small structural change results in drastic changes in uptake and localization of the compounds.

It should be noted, however, that mitochondrial accumulation is not always associated with non-selective toxicity. The presence of the HDPA ligand enhances and accelerates uptake significantly, and even leads to increased mitochondrial accumulation, yet complexes containing HDPA show high selective biological activities. In fact, it has

recently been reported that changes in polarity can affect whether mitochondria-targeted peptides simply accumulate in the mitochondrial matrix or disrupt the mitochondrial membrane activity and result in apoptosis.³⁶ Furthermore, while the antimetabolite methotrexate normally exhibits toxicity toward mammalian cells, when it is conjugated to a mitochondrial penetrating peptide, the altered subcellular localization reduces its toxicity by 3 orders of magnitude.³⁷

2.4.5 General Implications for Design

This work supports the hypothesis that nuclear DNA mismatch binding is responsible for the unique cell-selective biological activity of our rhodium metalloinsertors. Indeed, out of ten compounds studied, all ten exhibit sufficient nuclear uptake for mismatch binding. Furthermore, the fact that the three compounds that are not selective for the MMR-deficient cell line have enhanced mitochondrial accumulation implies that mitochondrial mismatch DNA targeting is not responsible for cell-selective behavior (**Figure 2.13**). As the only difference between the two cell lines is a functional copy of the MLH1 gene, a gene that encodes for a nuclear MMR protein, the cell-selective behavior of our metalloinsertors must be related to this MMR deficiency. As the mitochondria are the location of oxidative phosphorylation, where reactive oxygen species are unavoidably formed as byproducts, mitochondrial DNA has higher levels of oxidative damage than nuclear DNA.³⁸ While these DNA defects could very well be targets of our metalloinsertors, mtDNA repair pathways do exist,³⁹ and in most cases are distinct from their nuclear counterparts.⁴⁰ Specifically, the mitochondrial MMR proteins MSH2, MSH3, MSH6, and MLH1 have been shown to be absent from the

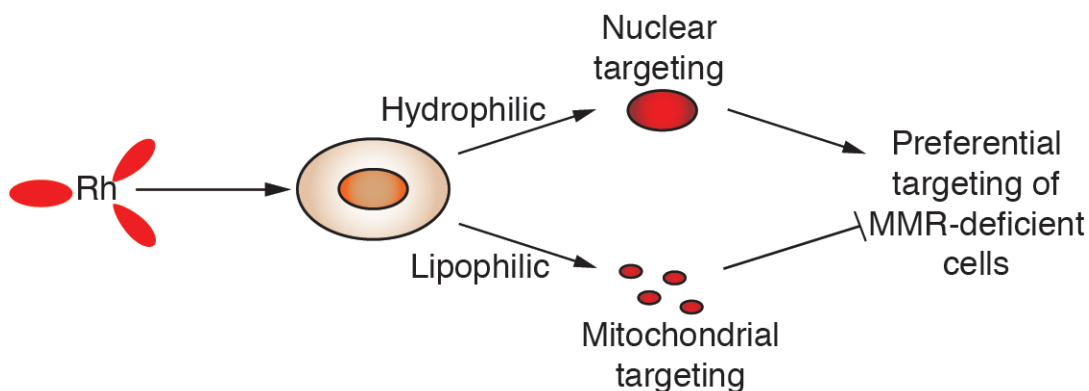


Figure 2.13 Model for the requirements for cell-selective targeting of MMR-deficient cells by rhodium metalloinsertors. All metalloinsertors localize to the nucleus in concentrations sufficient for mismatch binding. Mismatch recognition in genomic DNA is postulated as the preferred biological target of metalloinsertors for cell-selective biological activity in MMR-deficient cells. Complexes bearing lipophilic ancillary ligands also exhibit high mitochondrial uptake, which abolishes any selective effects and induces nonspecific cell death.

mitochondria.⁴¹ The targeting of defects in mitochondrial DNA therefore cannot be responsible for the unique cell-selective behavior of our metalloinsertors.

2.5 Conclusions

This work shows that in general, more extranuclear rhodium leads to nonselective biological activity. All compounds tested are present in the nucleus at sufficient concentrations for mismatch detection. However, the more lipophilic compounds, which display enhanced uptake into the cells, tend to localize more in the mitochondria, thus giving rise to nonspecific biological activity. While the more polar compounds ($[\text{Rh}(\text{NH}_3)_4(\text{phzi})]^{3+}$, $[\text{Rh}(\text{chrysi})(\text{phen})(\text{DPE})]^{2+}$, and $[\text{Rh}(\text{DPAE})_2(\text{chrysi})]^{3+}$) do not have the largest amount of cellular rhodium, there is consequently a smaller amount of rhodium in the mitochondria. This, coupled with sufficient nuclear rhodium for mismatch binding, gives rise to high MMR-deficient cell-selective biological activities for these three compounds. It seems that by increasing lipophilicity in an effort to increase uptake via passive diffusion, the subcellular localization is altered, leading to a larger amount of cellular rhodium residing in the mitochondria and less selectivity for the MMR-deficient cell line. This tradeoff in uptake for selectivity is in contrast to current strategies to improve the efficacy of cisplatin by increasing uptake of the drug.^{42,43} More generally, these results highlight that the relative accumulation of complex in different organelles needs to be considered, not simply cellular accumulation.

Most importantly, these data support the notion that the cell-specific activity we observe is caused by nuclear DNA mismatch targeting by our metalloinsertors. This exciting new result gives us key information in designing the next generation of rhodium metalloinsertors as cell-specific chemotherapeutics.

3.6 References

- 1 Wildenberg J., Meselson M. *Proc. Natl. Acad. Sci. USA*. **1975**, 72, 2202-2206.
- 2 Wagner, R. Jr., Meselson M. *Proc. Natl. Acad. Sci. USA*. **1976**, 73, 4135-4139.
- 3 Iyer, R. R., Pluciennik, A., Burdett, V. Modrich, P. L. *Chem. Rev.* **2006**, 106, 302-323.
- 4 Parsons, R., Li, G.-M., Longley, M., Modrich, P., Liu, B., Berk, T., Hamilton, S. R., Kinzler, K. W., Vogelstein, B. *Science*. **1995**, 268, 738-740.
- 5 Fink, D., Aebi, S., Howell, S. B. *Clin. Cancer Res.* **1998**, 4, 1-6.
- 6 Fram, R. J., Cusick, P. S., Wilson, J. M., Marinus, M. G. *Mol. Pharmacol.* **1985**, 28, 51-55.
- 7 Zeglis, B. M., Pierre, V. C., Barton, J. K. *Chem. Comm.* **2007**, 44, 4565-4579.
- 8 Jackson, B. A., Barton, J. K. *J. Am. Chem. Soc.* **1997**, 119, 12986-12987.
- 9 Jackson, B. A., Alekseyev, V. Y., Barton, J. K. *Biochemistry*. **1999**, 38, 4655-4662.
- 10 Jackson, B. A., Barton, J. K. *Biochemistry*. **2000**, 39, 6176-6182.
- 11 Keilkopf, C. L., Erkkila, K. E., Hudson, B. P., Barton, J. K., Rees, D. C. *Nat. Struct. Biol.* **2000**, 7, 117-121.
- 12 Pierre, V. C., Kaiser, J. T., Barton, J. K. *Proc. Natl. Acad. Sci. USA*. **2007**, 104, 429-434.
- 13 Zeglis, B. M., Pierre, V. C., Kaiser, J. T., Barton, J. K. *Biochemistry*. **2009**, 48, 4247-4253.
- 14 Song, H., Kaiser, J. T., Barton, J. K. *Nat. Chem.* **2012**, 4, 615-620.
- 15 Hart, J. R., Glebov, O., Ernst, R. J., Kirsch, I. R., Barton, J. K. *Proc. Natl. Acad. Sci. USA*. **2006**, 103, 15359-15363.

- 16 Ernst, R. J., Song, H., Barton, J. K. *J. Am. Chem. Soc.* **2009**, *131*, 2359-2366.
- 17 Ernst, R. J., Komor, A. C., Barton, J. K. *Biochemistry*, **2011**, *50*, 10919-10928.
- 18 Koi, M., Umar, A., Chauhan, D. P., Cherian, S. P., Carethers, J. M., Kunkel, T. A., Boland, C. R. *Cancer Res.* **1994**, *54*, 4308-4312.
- 19 Komor, A. C.; Schneider, C. J.; Weidmann, A. G.; Barton, J. K. *J. Am. Chem. Soc.* **2012**, *134*, 19223-19233.
- 20 Kirin, S. I., Yennawar, H. P., Williams, M. E. *Eur. J. Inorg. Chem.* **2007**, 3686-3694.
- 21 Gratzner, H. G. *Science*. **1982**, *218*, 474-475.
- 22 Mosmann, T. *J. Immunol. Methods*. **1983**, *65*, 55-63.
- 23 Zeglis, B. M., Barton, J. K. *Nature Protoc.* **2007**, *2*, 357-371.
- 24 Smith, P. K., Krohn, R.I., Hermanson, G.T., Mallia, A.K., Gartner, F.H., Provenzano, M.D., Fujimoto, E.K., Goeke, N.M., Olson, B.J., Klenk, D.C. *Anal. Biochem.* **1985**, *150*, 76-85.
- 25 Ahmad, K. A., Iskandar, J. L., Hirpara, K. B., Clement, M-V., Pervaiz, S. *Cancer Res.* **2004**, *64*, 7867-7878.
- 26 Wagner, B. K., Kitami, T., Gilbert, T. J., Peck, D., Ramanathan, A., Schreiber, S. L., Golub, T. R., Mootha, V. K. *Nat. Biotechnol.* **2008**, *26*, 343-351.
- 27 Yakes, F. M., Van Houten, B. *Proc. Natl. Acad. Sci. USA.* **1997**, *94*, 514-519.
- 28 Madesh, M., Bhaskar, L., Balasubramanian, K. A. *Mol. Cell. Biochem.* **1997**, *167*, 81-87.
- 29 Puckett, C. A.; Barton, J. K. *J. Am. Chem. Soc.* **2007**, *129*, 46-47.
- 30 Puckett, C. A.; Barton, J. K. *Biochemistry* **2008**, *47*, 11711-11716.

- 31 Fujioka, A.; Terai, K.; Itoh, R. E.; Aoki, N.; Nakamura, T.; Kuroda, S.; Nishida, E.; Matsuda, M. *J. Biol. Chem.* **2006**, *281*, 8917-8926.
- 32 Zhang, Y.; Lo, K. K-W. *Inorg. Chem.* **2009**, *48*, 6011-6025.
- 33 Candeil, L.; Gourdier, I.; Peyron, D.; Vezzio, N.; Copois, V.; Bibeau, F.; Orsetti, B.; Scheffer, G. L.; Ychou, M.; Khan, Q. A.; Pommier, Y.; Pau, B.; Martineau, P.; Del Rio, M. *Int. J. Cancer* **2004**, *109*, 848-854.
34. Eckford, P. D. W.; Sharom, F. J. *Chem. Rev.* **2009**, *109*, 2989-3011.
- 35 Fink, D.; Nebel, S.; Aebi, S.; Zheng, H.; Kim, H. K.; Christen, R. D.; Howell, S. B. *Cancer* **1997**, *76*, 890-893.
- 36 Horton, K. L.; Pereira, M. P.; Stewart, K. M.; Fonseca, S. B.; Kelley, S. O. *ChemBioChem.* **2012**, *13*, 476-485.
- 37 Pereira, M. P.; Kelley, S. O. *J. Am. Chem. Soc.* **2011**, *133*, 3260-3263.
- 38 Yakes, F. M.; Van Houten, B. *Proc. Natl. Acad. Sci. USA* 1997, *94*, 514-519.
- 39 Tomkinson, A. E.; Bonk, R. T.; Linn, S. *J. Biol. Chem.* **1988**, *263*, 12532-12537.
- 40 Liu, P.; Demple, B. *Environ. Mol. Mutagen.* **2010**, *51*, 417-426.
- 41 de Souza-Pinto, N. C.; Mason, P. A.; Hashiguchi, K.; Weissman, L.; Tian, J.; Guay, D.; Lebel, M.; Stevensner, T. V.; Rasmussen, L. J.; Bohr, V. A. *DNA Repair* **2009**, *8*, 704-719.
- 42 Fuertes, M. A.; Alonso, C.; Perez, J. M. *Chem. Rev.* **2003**, *103*, 645-662.
- 43 Gately, D. P.; Howell, S. B. *Br. J. Cancer* **1993**, *67*, 1171-1176.